

DOI: 10.1021/acscchemneuro.8b00600

**Brain Penetrable Histone Deacetylase 6 Inhibitor SW-100
Ameliorates Memory and Learning Impairments in a Mouse
Model of Fragile X Syndrome**

Journal:	<i>ACS Chemical Neuroscience</i>
Manuscript ID	cn-2018-00600y.R1
Manuscript Type:	Article
Date Submitted by the Author:	27-Nov-2018
Complete List of Authors:	KOZIKOWSKI, ALAN; StarWise Therapeutics LLC, Shen, Sida; Northwestern University, Chemistry Pardo, Marta; University of Miami, Miller School of Medicine, Department of Neurology Tavares, Mauricio; Universidade de Sao Paulo Faculdade de Ciencias Farmaceuticas, Pharmacy Szarics, Dora; University Health Network Benoy, Veronick; KU Leuven, VRC & VIB, Zimprich, Chad; Promega Corp, R&D Cellular Analysis Kutil, Zsofia; Akademie Ved Ceske Republiky Ustav Experimentalni Botaniky, Laboratory of Plant Biotechnologies Zhang, GuiPing; University of Illinois at Chicago College of Medicine, Department of Medicinal Chemistry and Pharmacognosy Barinka, Cyril; Institute of Biotechnology ASCR, Laboratory of Structural Biology Robers, Matthew; Promega Corp, Research and Development Van Den Bosch, Ludo; Vesalius Research Center, Laboratory for Neurobiology Eubanks, James; University Health Network Jope, Richard; University of Miami, Miller School of Medicine

SCHOLARONE™
Manuscripts

1
2
3
4
5
6
7 **Brain Penetrable Histone Deacetylase 6 Inhibitor SW-100 Ameliorates**
8
9 **Memory and Learning Impairments in a Mouse Model of Fragile X Syndrome**
10
11

12 Alan P. Kozikowski^{1,*}, Sida Shen^{2,‡,†}, Marta Pardo^{3,‡,†}, Maurício T. Tavares^{2,†}, Dora Szarics⁴,
13 Veronick Benoy⁵, Chad A. Zimprich⁶, Zsófia Kutil⁷, Guiping Zhang², Cyril Bařinka⁷, Matthew
14 B. Robers⁶, Ludo Van Den Bosch⁵, James H. Eubanks⁴, & Richard S. Jope³
15
16
17
18
19

20
21 ¹ StarWise Therapeutics LLC, Madison, WI 53719, United States
22

23
24 ² Department of Medicinal Chemistry and Pharmacognosy, College of Pharmacy, University of
25 Illinois at Chicago, Chicago, IL 60612, United States
26
27

28
29
30 ³ Department of Psychiatry and Behavioral Sciences, Miller School of Medicine, University of
31 Miami, Miami, FL 33136, United States
32
33

34
35 ⁴ Division of Genetics and Development, Krembil Research Institute, University Health
36 Network, Toronto, Ontario M5G 2C4, Canada
37
38

39
40
41 ⁵ Laboratory of Neurobiology, Vesalius Research Center (VIB) and Leuven Research Institute
42 for Neuroscience and Disease (LIND), KU Leuven, B-3000 Leuven, Belgium.
43
44

45
46 ⁶ Promega Corporation, Madison, WI 53711, United States.
47
48

49
50 ⁷ Laboratory of Structural Biology, Institute of Biotechnology of the Czech Academy of
51 Sciences, Prumyslova 595, 252 50 Vestec, Czech Republic
52
53
54
55
56
57
58
59
60

ABSTRACT

Disease-modifying therapies are needed for Fragile X syndrome (FXS), as at present there are no effective treatments or cures. Herein, we report on a tetrahydroquinoline-based selective histone deacetylase 6 (HDAC6) inhibitor SW-100, its pharmacological and ADMET properties, and its ability to improve upon memory performance in a mouse model of FXS, *Fmr1*^{-/-} mice. This small molecule demonstrates good brain penetrance, low-nanomolar potency for the inhibition of HDAC6 (IC₅₀ = 2.3 nM), with at least a thousand-fold selectivity over all other class I, II, and IV HDAC isoforms. Moreover, through its inhibition of the α -tubulin deacetylase domain of HDAC6 (CD2), in cells SW-100 upregulates α -tubulin acetylation with no effect on histone acetylation and selectively restores the impaired acetylated α -tubulin levels in the hippocampus of *Fmr1*^{-/-} mice. Lastly, SW-100 ameliorates several memory and learning impairments in *Fmr1*^{-/-} mice, thus modeling the intellectual deficiencies associated with FXS, and hence providing a strong rationale for pursuing HDAC6-based therapies for the treatment of this rare disease.

KEYWORDS phenylhydroxamate, permeability, Ames negative, acetylated α -tubulin, memory and learning impairments

INTRODUCTION

Fragile X Syndrome (FXS) is the most common form of inherited severe cognitive impairment in males (1 in 3,000 to 4,000 individuals) and a significant cause of intellectual disability in females (1 in 7,000 to 8,000 individuals).¹ This condition causes an array of developmental problems including learning disability, cognitive impairment, and behavioral characteristics. Other signs and symptoms may include autism spectrum disorders, seizures, and characteristic physical features. In most cases, FXS is caused by transcriptional silencing of the fragile X mental retardation 1 (*FMR1*) gene due to the methylation of a cytosine-guanine-guanine (CGG) trinucleotide repeat expansion (number of repeats in FXS > 200, normal < 50),² resulting in the absence of the gene product, fragile X mental retardation protein (FMRP) which regulates mRNA trafficking and dendritic translation. FMRP deficiency affects the translational regulation of multiple proteins, including several that are important for learning and memory.³⁻⁵ At present, there are no effective treatments or cures for FXS. Metabotropic glutamate receptor 5 (mGlu5) inhibitors were considered as a potential therapy for FXS based on the ‘mGluR theory of FXS’.⁶⁻⁸ Recent phase II clinical trials, however, with two different mGlu5 negative allosteric modulators (basimglurant and mavoglurant) failed to induce significant improvement over placebo for primary endpoints.^{9, 10} In addition to mGluR5, a diverse set of alternative therapeutic targets such as GSK-3 β , ERK1/2, IGF1, and MMP9 have been investigated in animal studies or early clinical trials.¹¹ Among them, the pan-histone deacetylase (HDAC) inhibitor valproic acid (VPA) was found to ameliorate the symptoms of attention deficit hyperactivity disorder (ADHD) in FXS boys.¹² After VPA treatment in FXS lymphoblastoid cells, however, FMR1-mRNA levels remained low, FMRP protein was undetectable, and the gene remained methylated, although a significant increase in histone acetylation was observed.¹³ Additionally, there is accumulating evidence that the down-

1
2
3 regulation of class I and II HDAC levels leads to neuroprotection or improvement of learning and
4 memory in rodent models of various brain diseases.¹⁴⁻¹⁸ Some research studies have demonstrated,
5
6 for example, that the administration of siRNA targeting class I HDACs 1-3, which are
7
8 predominantly responsible for regulating histone acetylation, improves cognitive impairments in
9
10 the FXS intellectual deficiency mouse model.¹⁹ However, to date no research has been published
11
12 on the activity of selective HDAC6 inhibitors in FXS animal models.
13
14
15

16
17 Histone deacetylases (HDACs) are a family of proteins responsible for catalyzing the hydrolysis
18
19 of acetylated histone lysine residues to produce deacetylated products. There are 18 known
20
21 mammalian HDACs, which are divided into 4 classes, based on their sequence similarity to yeast
22
23 homologs: class I (HDAC1, 2, 3, and 8), class IIa (HDAC4, 5, 7, and 9), class IIb (HDAC6 and
24
25 10), class III (SIRT1-7), and class IV (HDAC11).²⁰ Among these isoforms, HDAC6 has attracted
26
27 particular attention due to its relative uniqueness within its family: (a) unlike its related class
28
29 members, HDAC6 contains two tandem protein deacetylase motifs (CD1 and CD2) and has an *N*-
30
31 terminal nuclear export sequence and a *C*-terminal cytoplasmic retention sequence;^{21, 22} (b) unlike
32
33 other HDAC members, which are present in the nucleus, HDAC6 is found primarily within the
34
35 cytosol and is responsible for regulating the acetylation state of specific cytosolic proteins,
36
37 although it is also able to shuttle into the nucleus and thus can also potentially regulate
38
39 transcription.²³ Its regulation of α -tubulin acetylation has sparked considerable interest because
40
41 microtubule-dependent transport rates are facilitated by higher levels of acetylated α -tubulin.²⁴⁻²⁷
42
43 This effect presumably stems from the increased association of the motor proteins kinesin-1 and
44
45 dynein with acetylated α -tubulin, which in turn regulates both anterograde and retrograde transport
46
47 activities.²⁸ In addition to facilitating anterograde transport of new cargo to synaptic zones,
48
49 acetylated α -tubulin also increases the ability of damaged organelles or misfolded proteins to leave
50
51
52
53
54
55
56
57
58
59
60

1
2
3 synaptic zones.²⁹ Selective inhibition of HDAC6 thus appears to offer a potential therapeutic
4 approach for treating a number of neurological disorders such as depression,³⁰ stroke,³¹
5 Parkinson's disease,³² Alzheimer's disease,³³⁻³⁵ Charcot-Marie-Tooth disease,³⁶⁻³⁸ Rett
6 Syndrome,^{33, 39} and amyotrophic lateral sclerosis (ALS).⁴⁰ Intriguingly, significantly fewer
7 mitochondria and greatly reduced mitochondrial mobility have been observed in hippocampal
8 neurites of Fragile-X-associated tremor/ataxia syndrome (FXTAS, 50 < number of CGG repeats
9 < 200).^{41, 42} Since HDAC6 inhibitors have been shown to increase mitochondrial movement
10 including vesicular trafficking of brain-derived neurotrophic factor (BDNF),⁴³⁻⁴⁵ we postulated
11 that HDAC6 inhibition could provide a useful therapeutic intervention for FXS. Therefore, an
12 early aim of the present study was to investigate whether selective inhibition of HDAC6 could
13 increase the acetylation of α -tubulin in brain, and if so whether that modification would improve
14 the FXS-like phenotypes in *Fmr1*^{-/-} mice.

15
16
17
18
19
20
21
22
23
24
25
26
27
28
29
30
31 A number of broad-spectrum HDAC inhibitors, such as vorinostat (SAHA), romidepsin,
32 panobinostat, and belinostat, are being used as anti-cancer agents due to their ability to enhance
33 gene expression by increasing histone acetylation, and in turn promoting cell-cycle arrest,
34 differentiation, and apoptosis. However, significant concerns have emerged that pan-HDAC
35 inhibitors may be too broadly acting for clinical use beyond oncology, especially with respect to
36 their potential neurotoxicity.^{46, 47} In the last decade, selective HDAC6 inhibitors (HDAC6is) have
37 been reported,⁴⁸ and two (poorly selective) HDAC6is (rocilinostat and citarinostat) are in clinical
38 trials for several types of cancer.⁴⁹⁻⁵¹ However, only a handful of HDAC6is have been reported
39 that are brain-penetrant and display appropriate *in vitro* and *in vivo* activities in models of
40 neurological diseases.^{30, 52-55}

1
2
3 One selective HDAC6i discovered by our group, tubastatin A (TubA), has been investigated for
4 its potential to be used in central nervous system (CNS) disorders.^{30-35, 39, 44} TubA exhibits four of
5 the six desirable physicochemical properties for CNS drugs within the predicted optimal ranges:
6 tPSA ($40 < \text{tPSA} \leq 90 \text{ \AA}^2$), pK_a (≤ 8.0 , basic moiety), clogP (≤ 3), and MW (≤ 360), whereas two
7 parameters including its HBD (optimally = 0) and clogD (optimally ≤ 2) are in less favorable
8 ranges. As such, TubA receives a relatively high CNS multi-parameter optimization (MPO)
9 desirability score of 5.33 (>5).⁵⁶⁻⁵⁸ Moreover, the positive calculated logBB value of TubA (0.18,
10 determined by ACD/Percepta software) suggests that TubA should cross the blood-brain-barrier
11 (BBB) effectively. However, its measured ratio of brain to plasma levels has been reported to be
12 only modest ($\text{AUC}_{\text{brain}}/\text{AUC}_{\text{plasma}} = 0.18$).³⁰ Thus, prior to exploring the effects of an HDAC6i in
13 the FXS mouse model, we needed to identify a compound with improved brain penetration.
14
15
16
17
18
19
20
21
22
23
24
25
26
27

28 To better understand the reasons for the poor brain penetration of TubA, and to further guide the
29 identification of future novel brain penetrant analogs, we present here a set of HDAC6i analogs
30 selected from our compound library. Using a series of design modifications and *in vitro*
31 experiments we were able to identify the novel brain-penetrant HDAC6i, designated SW-100. This
32 compound is easy to synthesize, and it possesses low nanomolar potency against HDAC6,
33 excellent isozyme selectivity over other HDACs, selective engagement of HDAC6-CD2 as
34 measured in cells, as well as α -tubulin/histone acetylation selectivity in neurons. Moreover, we
35 were able to show that selective HDAC6i increases the levels of acetylated α -tubulin in the
36 hippocampus of *Fmr1*^{-/-} mice, and that this correlates with improved learning and memory
37 performances in this animal model of FXS.
38
39
40
41
42
43
44
45
46
47
48
49
50
51
52
53
54
55
56
57
58
59
60

RESULTS AND DISCUSSION

SW-100 is a highly selective and potent HDAC6 inhibitor

The structure of a typical HDACi consists of a cap that interacts with the surface of the catalytic cavity, a linker that occupies the hydrophobic channel, and a zinc binding group (ZBG) that coordinates with the zinc ion (Zn^{2+}) at the deep bottom of the pocket. In general, the phenylhydroxamate motif has been demonstrated to impart HDAC6 selectivity to a host of ligands, as first revealed by the invention of TubA. X-ray crystal structures of several related compounds in complex with HDAC6 typically display similar monodentate phenylhydroxamate- Zn^{2+} coordination geometry, while a canonical bidentate Zn^{2+} coordination was observed for the hydroxamate inhibitors that bear an alkyl chain in the linker region, as exemplified by the pan-HDAC inhibitor TSA and the partially selective, HDAC6i ricolinostat.⁵⁹ The two residues Phe583 and Phe643 located within the hydrophobic channel engage in a double π -stacking interaction with the phenyl group present in the linker.⁵⁹ A previous publication has reported that even the capless parent compound, phenylhydroxamate (**1**) (Figure 1a), shows an IC_{50} of 115 nM against HDAC6 and more than 10-fold selectivity over class I HDACs.⁶⁰ In this case, the crystal structure of the enzyme-inhibitor complex containing phenylhydroxamate also displays bidentate zinc coordination, which is believed to underly its high potency.⁶¹ Thus, the capping group attached to the phenylhydroxamate moiety is able to affect its degree of coordination with the catalytic Zn^{2+} ion leading to either bidentate or monodentate chelation. It has been calculated that the monodentate coordination mode is slightly less stable by ~ 0.5 kcal/mol compared to bidentate coordination.⁵⁹ Appendage of an *N,N*-diethylaminomethylene group or a pyrrolidinomethylene group on the phenylhydroxamic acid core leads to compounds **2** and **3**, respectively, both of which show reduced HDAC6 activity. On the other hand, the heteroaromatic pyrrolomethylene (**4**) and

1
2
3 indolylmethylene (**5**) derivatives, which can be viewed as structurally simplified analogs of TubA,
4
5 provide analogs of nanomolar activity against HDAC6 and high selectivity over HDAC1 (Figure
6
7 1a).⁶² Docking simulations of compounds **2–5** and TubA to the active site of HDAC6-CD2 (Figure
8
9 1b-f) have been carried out, and these studies reveal that **2**, **4**, and TubA engage in monodentate
10
11 coordination with Zn²⁺, with binding being further enhanced by hydrogen bonding interactions
12
13 with Gly582 and Tyr745 (**2**, Figure 1c); Gly582 and His614 (**4**, Figure 1d); or Gly582, Cys584,
14
15 and Tyr745 (TubA, Figure 1e), respectively. Within the narrow hydrophobic channel of HDAC6-
16
17 CD2, Phe583 and Phe643 engage in double π -stacking interactions with the bulky phenyl group
18
19 present in the linker; this binding mode is consistent with the interactions observed from the X-ray
20
21 structure of the phenylhydroxamate **1** in complex with HDAC6.⁶⁰ The *N,N*-diethylamino group
22
23 of **2** did not show any hydrophobic interactions with the rim region, while the pyrrole cap of **4** was
24
25 found to engage in a hydrophobic interaction with the Pro464 side chain (Figure 1c), which is
26
27 similar to that observed for the tricyclic moiety of TubA (Figure 1e). Overall, hydrophobic
28
29 interactions between the aromatic caps and the residues present on the rim region of HDAC6
30
31 provide additional binding energies, regardless of the size of these cap groups. This information
32
33 may be helpful in the design of other novel ligands that may in turn show an improved ability to
34
35 penetrate the blood-brain-barrier.
36
37
38
39
40
41
42
43
44
45
46
47
48
49
50
51
52
53
54
55
56
57
58
59
60

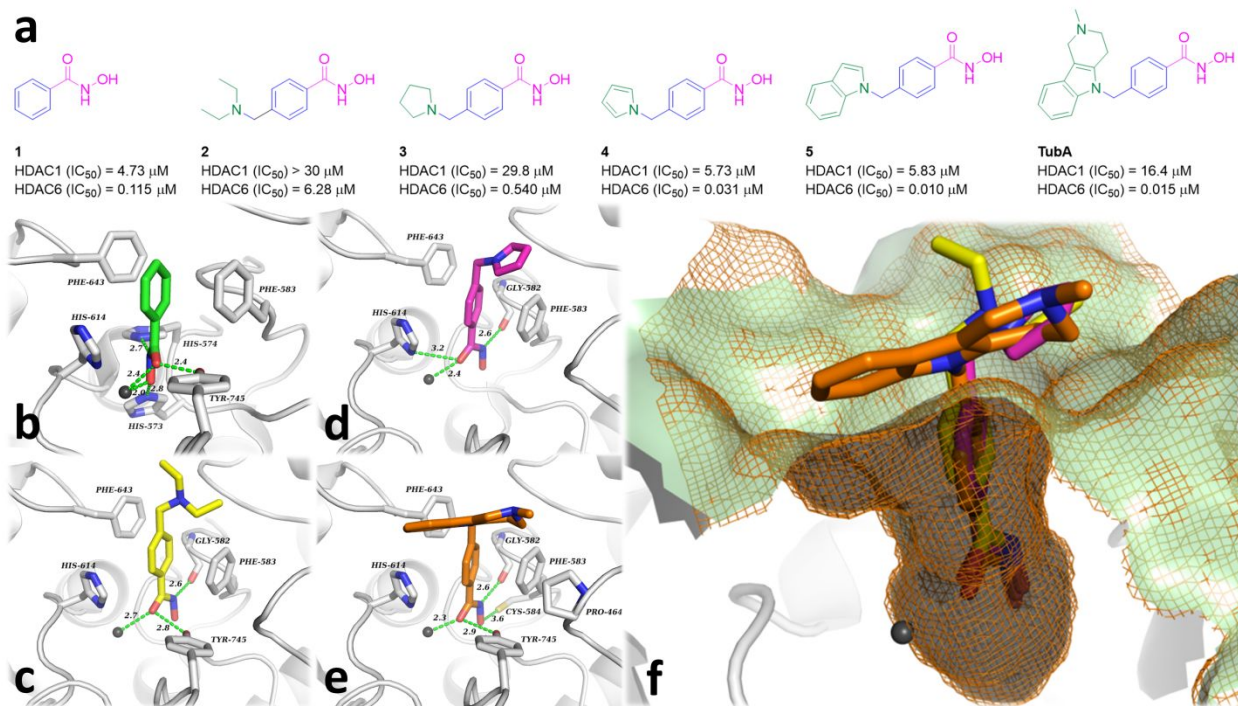
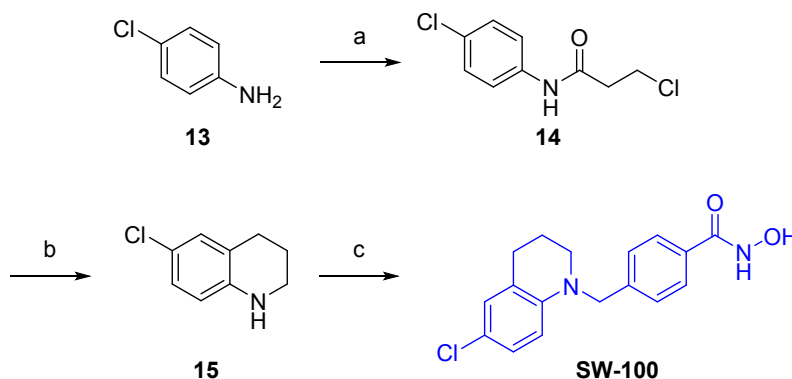


Figure 1. Hydrophobic caps are valuable for enhancing HDAC6 potency. (a) HDAC1/6 enzyme potencies and structures of compounds **1-5**; (b) Empirical conformation of **1** (green) in HDAC6-CD2 (PDB: 6CSR); (c-e) Docked pose of **2** (yellow), **4** (magenta), and TubA (orange) in HDAC6-CD2; (f) Superimposed structures of **2**, **4**, and TubA in the catalytic site of HDAC6-CD2. Interatomic distances of both polar interactions and coordination are depicted in green dashed lines (distance in Å). Zn^{2+} ions are depicted as dark grey spheres. The mesh molecular surface is depicted in orange (wires) and pale green (surface).

Next we selected several HDAC6is containing different types of monocyclic or bicyclic aromatic caps from our work for further investigation (Figure 2a).^{62, 63} The majority of these compounds exhibit desirable calculated CNS physicochemical properties and MPO scores that would suggest ready brain permeability (Table S1).⁵⁸ TubA and another well-known HDAC6i NexA⁶⁴ were included as positive controls. A number of these potent HDAC6is including TubA and NexA exhibit high selectivity against the class I HDACs 1, 2, and 3 but poorer selectivity

1
2
3 against HDAC8 (Figure 2b and 2c). The benzimidazole analogs **8** and **9** were also found to show
4 strong activity against the class IIa isoforms. On the other hand, based upon these data and other
5 SAR data available to us, we designed the tetrahydroquinoline (THQ)-based analog SW-100. The
6 synthetic route to SW-100 starts from 4-chloroaniline (**13**) which was first converted to the N-
7 phenylpropanamide **14** by treatment with 3-chloropropanoyl chloride. Next, intramolecular
8 Friedel-Crafts cyclization using aluminum trichloride followed by reduction of the intermediate
9 lactam with LiAlH₄ afforded the tetrahydroquinoline **15**. The building block **15** was then alkylated
10 with commercially available methyl 4-(bromomethyl)benzoate to provide the corresponding ester,
11 which upon treatment with an aqueous NH₂OH/NaOH solution afforded the desired hydroxamate
12 analog SW-100 (Scheme 1). The chemical route has been used to prepare multigram amounts of
13 this HDAC6i.
14
15
16
17
18
19
20
21
22
23
24
25
26
27



Scheme 1. Reagents and conditions. a) 3-chloropropanoyl chloride, acetone, reflux; b) (i) AlCl₃, 140 °C (neat), (ii) LiAlH₄, THF, 0 °C to reflux; c) (i) methyl 4-(bromomethyl)benzoate, K₂CO₃, DMF, 100 °C, (ii) NaOH, 50 wt% aq. NH₂OH, THF/MeOH (1:1), 0 °C to rt.

As apparent from the data presented in Figure 2, SW-100 exhibits a 1000-fold to 10000-fold selectivity for HDAC6 relative to all other HDAC isozymes, including HDAC8 (SI: 1280-fold; data from Reaction Biology Corp.).

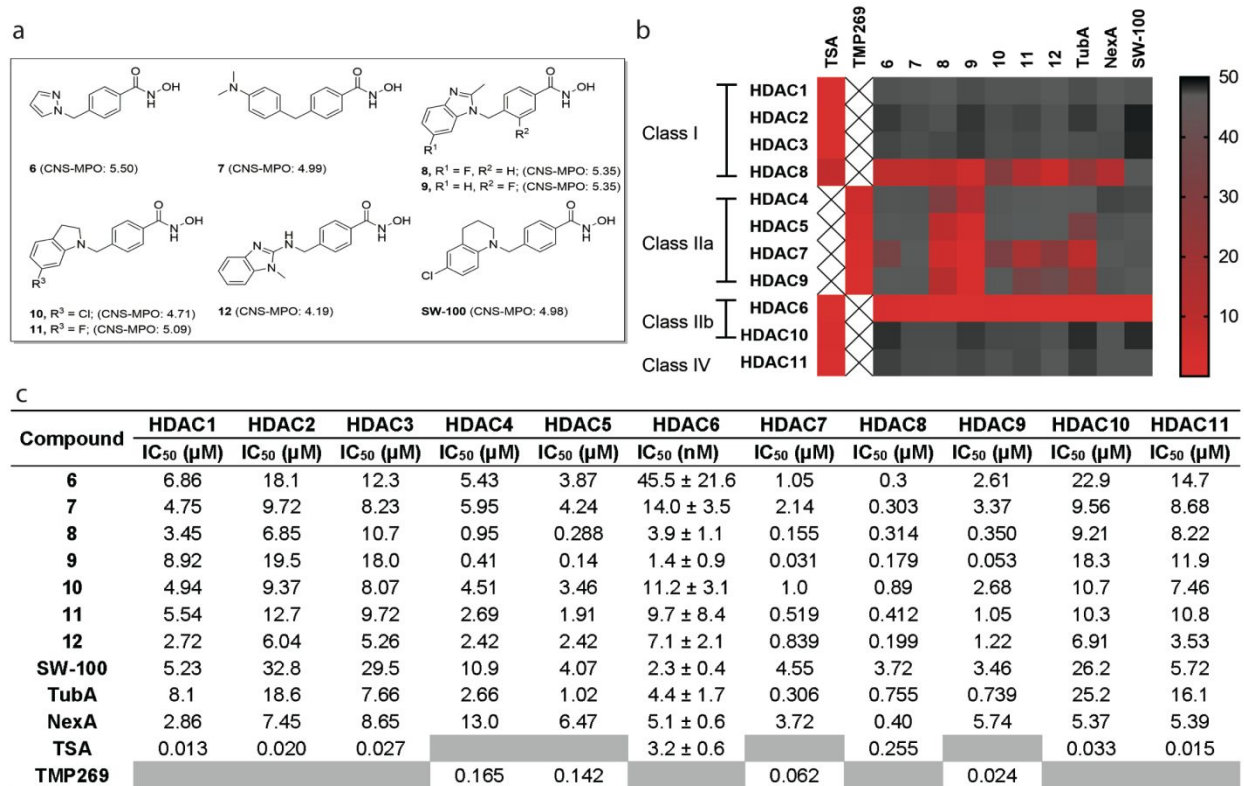
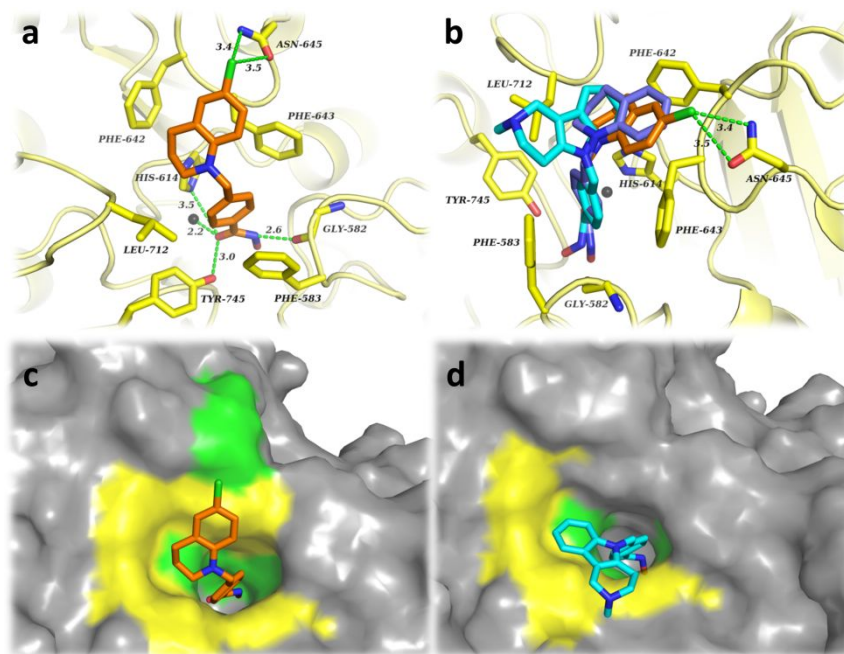


Figure 2. SW-100 is a highly potent and selective HDAC6 inhibitor. (a) Structures of compounds **6-12**, and SW-100; (b) Heatmap summary of HDAC activities; (c) Full HDAC potency table of SW-100, TubA, and NexA. IC₅₀ values are the mean of two experiments ± SD obtained from curve-fitting of a 10-point enzymatic assay starting from 30 μM with 3-fold serial dilution against all HDAC isoform; TSA was tested in singlet 10-dose IC₅₀ mode with 3-fold serial dilution starting at a concentration of 10 μM against HDAC class I, IIb, and IV isoforms; TMP269, a selective HDAC class IIa inhibitor, was tested in singlet 10-dose IC₅₀ mode with 3-fold serial dilution starting at a concentration of 10 μM against HDAC class IIa isoforms.

The docking results of SW-100 with HDAC6-CD2 shown in Figure 3 indicate that the hydroxamate group engages in the expected monodentate interaction with the Zn²⁺ ion, which is further reinforced by hydrogen bonding between its NH and the Gly582 backbone as well as the carbonyl and Tyr745/His614, respectively. Both residues Phe583 and Phe643 located in the

1
2
3 hydrophobic channel engage in double π -stacking interactions with the phenyl ring present in the
4 linker of SW-100. Also, an additional interaction was observed between the chlorine atom on the
5 linker of SW-100. Also, an additional interaction was observed between the chlorine atom on the
6 THQ cap and Asn645 present on the rim of the HDAC6-CD2 pocket (Figure 3a). Superimposed
7 and surface views of SW-100 and TubA in Figure 3b-d show that TubA engages in hydrophobic
8 interactions with Leu712 while SW-100 is turned toward residues Phe642 and Asn645. From
9 these static images, it is clear that the cap groups add to inhibitor potency through interactions with
10 different residues comprising the large rim area. Moreover, in comparison with the parent THQ
11 analog **16** [blue ligand in Figure 3b which lacks the chlorine atom; structure shown in Figure S2,
12 IC_{50} (HDAC6) = 15 nM],⁶² SW-100 rotates within the binding pocket to allow for the interaction
13 with Asn645 at the rim surface which may in turn be responsible for the improved potency of SW-
14 100.



29
30
31
32
33
34
35
36
37
38
39
40
41
42
43
44
45
46
47
48
49
50
51 **Figure 3** (a) Binding interactions of SW-100 (orange) within the HDAC6-CD2; (b) Superimposed
52 structures of SW-100 (orange), **16** (blue), and TubA (cyan) with HDAC6-CD2; (c) Surface pose
53 of SW-100 (orange) within HDAC6-CD2; (d) Surface pose of TubA (cyan) within HDAC6-CD2.

The Zn²⁺ ion is depicted as a grey sphere. Molecular surfaces are depicted in in grey, yellow (hydrophobic interaction area) and green (polar interaction area).

It is well appreciated that the ability of a small molecule to inhibit an enzyme in its pure/isolated state may not properly translate to its predicted outcomes in the cellular context. It thus became of interest to further assess the potency and selectivity of SW-100 in live cells using the NanoBRET target engagement assay, which is based on the competitive displacement of a luminescent reporter complex utilizing a cell-permeable SAHA tracer.⁶⁵ These results are summarized in Figures 4a-d, and demonstrate that SW-100 maintains high selectivity over HDAC1 in cells. The measured HDAC6 potency of SW-100 was slightly higher when the α -tubulin preferring deacetylase domain of HDAC6, the CD2 domain (IC₅₀ = 97 nM) was used in place of full-length HDAC6 (IC₅₀ = 279 nM). Results are also provided for SAHA for comparison purposes (Figure 4a-d).

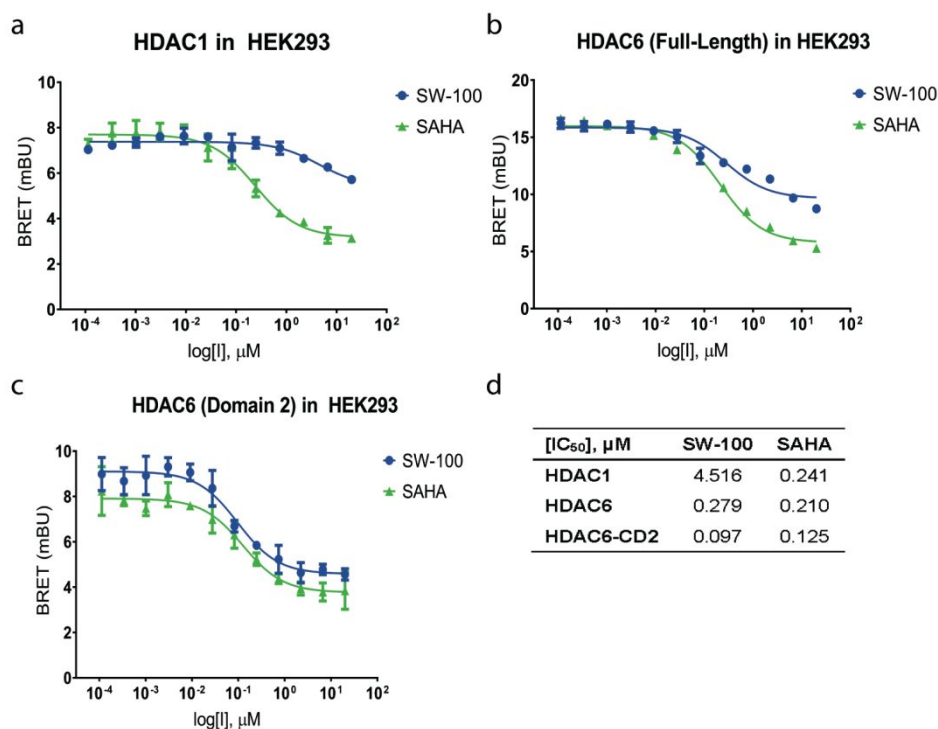


Figure 4. SW-100 selectively inhibits HDAC6-CD2 and enhances α -tubulin acetylation in cells. (a-d) HDAC1/6 NanoBRET target engagement assay for compound SW-100 in HEK293. IC_{50} values are the mean of four experiments \pm SEM obtained from curve-fitting of a 12-point engagement assay starting from a concentration of 20 μ M with 3-fold serial dilution. SAHA was used as a positive control.

SW-100 displays a significantly improved ability to cross the blood-brain-barrier

A compound's brain uptake is largely determined by its ability to diffuse over cellular membranes and its affinity for drug efflux transporters like P-glycoprotein (P-gp), which is extensively expressed at the BBB.⁶⁶ Compounds with permeability coefficients [$P_{app(A-B)}$] higher than 3×10^{-6} cm/s generally show high brain uptake, while compounds with $P_{app(A-B)}$ less than 1×10^{-6} cm/s in the MDCK-MDR1 cell assay are less likely to penetrate the BBB.⁶⁷ The data in Table 1 reveal that all compounds studied can be classified as moderately permeable (2×10^{-6} cm/s $< P_{app(A-B)} < 20 \times 10^{-6}$ cm/s) except for the benzimidazole analog **12** that shows both a modest $P_{app(A-B)}$ and $P_{app(B-A)}$. All three benzimidazole analogs (**8**, **9**, and **12**) display unfavorable efflux ratios (>2.5) for CNS access as results from their higher $P_{app(B-A)}$.⁶⁸ Notably, the extremely high $P_{app(B-A)}$ of TubA results in an efflux ratio of 9.83, while compounds **6**, **7**, **10**, **11**, and SW-100 exhibit more favorable efflux ratios (<1.0). The predicted physicochemical properties and desirable CNS-MPO scores suggest that all these compounds should exhibit similar permeability properties (Table S1). However, diverse P-gp efflux ratios were obtained which may be related to the amphoteric properties of these inhibitors. The calculated pK_a values of the acidic hydroxamate groups are in the range of 9.0-9.2, while the pK_a values of basic functional group in the cap groups range from 0.84 to 7.14 (Table 1 and Figure S1). A zwitterionic form is a preferred protonation form for many amphoteric drugs at physiological pH, while a neutral status may become

predominant when the pK_a values of the basic moiety are lower than 3.⁶⁹ Moreover, the zwitterionic character of a compound usually leads to poor membrane permeability. However, this is amenable to improvement by replacing a more basic moiety with a less basic one.^{70, 71} We thus plotted the efflux ratios against the cap group's pK_a , and the observed correlation is consistent with the foregoing postulate (Figure S1). In light of the favorable cell line permeability data for SW-100, we next carried out brain/plasma PK studies *in vivo*. As apparent from the data presented in Table 2, SW-100 affords a reasonably good brain/plasma ratio of 2.44 at 1 h and 4.54 at 4 h upon IP administration in wild-type (WT) mice, data that are consistent with its low efflux ratio. In contrast, TubA displays a poor brain/plasma ratio of 0.15 at 8 min and 0.86 at 60 min after IV administration in WT mice which is consistent with its permeability properties (Table S2).

SW-100 was also evaluated in both liver microsomal and hepatocyte stability assays, as well as for hERG and CYP inhibition. The data in Table 2 indicate that its metabolic stability is low, while inhibition of the hERG and CYPs are generally in an acceptable range. In addition, to investigate the possible mutagenicity of SW-100,⁷² the compound was incubated with four strains of *Salmonella typhimurium* (TA98, TA100, TA1535, and TA1537) and one strain of *Escherichia coli* (WP2 uvrA) in the presence and absence of mammalian microsomal enzymes (S9 mix). The results in Table 2 show that SW-100 is negative under the conditions of this Ames assay.

Compd.	pK_a		MDCK-MDR1 cell line		
	acidic	basic	$P_{app (A-B)}$ (10^{-6} , cm/s)	$P_{app (B-A)}$ (10^{-6} , cm/s)	Efflux Ratio
SW-100	9.05	2.91	4.58	2.33	0.51
6	9.20	2.07	7.35	5.24	0.70
7	9.20	5.12	17.61	11.04	0.63
8	9.20	5.95	4.44	13.45	3.23

9	9.00	5.86	3.89	13.17	4.23
10	9.05	0.99	9.14	5.54	0.62
11	9.05	0.84	10.46	11.08	1.05
12	9.05	6.55	0.66	2.05	2.95
TubA	9.20	7.14	2.00	19.66	9.83

Table 1. Permeability determination for **6-12**, SW-100, and TubA.^a

^apK_a values were obtained by Marvin Sketch version 18.5. MDCK-MDR1 cell line assays were carried out by Pharmaron, Inc. (Irvine, CA).

Table 2. Brain/plasma pilot PK studies and initial ADMET evaluation of SW-100.^a

Brain/plasma PK studies					
route	dose (mg/kg)	time (h)	brain concentration (ng/mL)	plasma concentration (ng/mL)	brain/plasma ratio
IP	20	1	141.8 ± 52.3	58.2 ± 24.9	2.44
IP	20	4	11.5 ± 0.30	2.52 ± 0.13	4.54
ADMET parameters					
Liver microsomal stability (t _{1/2} min)				Human	23
				Mouse	23
Hepatocyte stability (t _{1/2} , min)				Human	30
				Mouse	10
hERG test (IC ₅₀ , μM)				HEK293 cells	12.23
CYP inhibition (%@10 μM)				1A2	20.53
				2C9	18.84
				2C19	83.21
				2D6	2.51
				3A4	-0.63

Ames test	TA98, TA100, TA1535, TA1537, WP2 <i>uvrA</i>	negative
-----------	---	----------

^aSW-100 was administered to C57BL/6 male mice by IP administration at the dose of 20 mg/kg. Blood and brain samples were collected at 1 h and 4 h time-points. Brain tissues were homogenized at a 1:4 ratio of tissue weight (g) to volume of PBS (mL). The data found (ng/mL) was multiplied by 5 to obtain the concentration (ng/mL) in brain tissues. PK studies and ADMET profiles were conducted by Pharmaron, Inc., Irvine, CA.

SW-100 selectively enhances the levels of acetylated α -tubulin *in vitro*.

Compounds **6**, **7**, **10**, **11**, and SW-100, having reasonable efflux ratios, were further evaluated for their ability to induce α -tubulin acetylation (Figure 5a-c) in cells. HEK293 cells were treated with the HDAC6i at concentrations of 0.01, 0.1, 1, and 10 μ M. As is apparent from the data displayed in Figure 5a the monocyclic analogs **6** and **7** were able to elevate the levels of acetylated α -tubulin only at concentrations of 10 μ M (one-way ANOVA $F(10,32) = 8.425, p < 0.0001$), while the indole analogs **10** and **11** began to show reasonable activity at 1 μ M (one-way ANOVA $F(10,22) = 5.973, p = 0.0002$, Figure 5b). In contrast, SW-100 treatment led to a more obvious increase in the acetylated α -tubulin levels in a dose-dependent manner that was similar to the results shown by the comparator compound NexA (one-way ANOVA $F(10,45) = 4.537, p = 0.0002$, Figure 5c). Further, in order to ascertain the functional selectivity of SW-100, we assessed its ability to induce histone acetylation in comparison to tubulin acetylation in the N2a cells. As is apparent from the bar graphs in Figures 5d-f, SW-100 increased the ratio of acetylated α -tubulin to α -tubulin (>8-fold compared to vehicle, $p = 0.07$) while inducing only modest changes in the levels of acetylated histone 3 to histone 4 (<1.5-fold compared to vehicle). These effects are similar to those found for the reference HDAC6i TubA (one-way ANOVA, $F(3,12) = 3.272, p = 0.05$) at

1 μM . In contrast, the pan-active HDACi TSA increased levels of both acetylated α -tubulin and acetylated histone H3 significantly compared to vehicle ($p < 0.01$, Figure 5a and 5c).

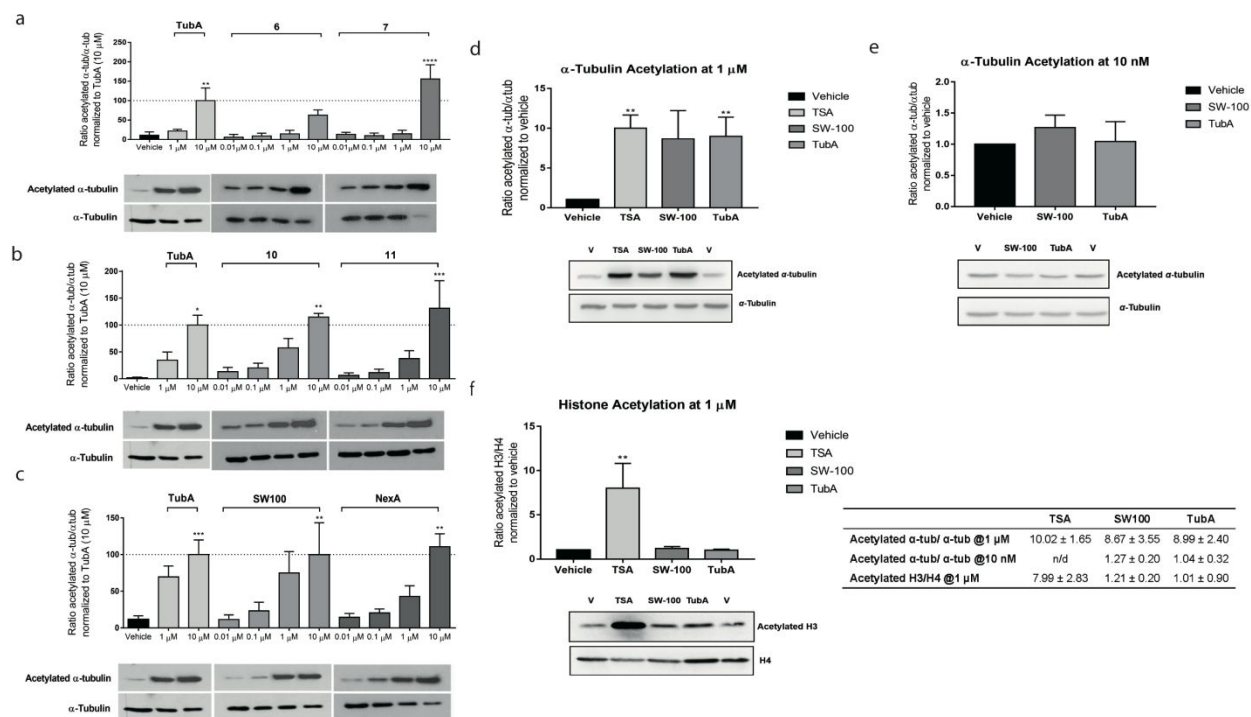


Figure 5. SW-100 increases the levels of acetylated α -tubulin in a dose-dependent manner in HEK293 cells (a-c) and selectively increases the levels of acetylated α -tubulin in N2a cells (d-f). (a-c) The α -tubulin acetylation assay was carried out in HEK293 cells treated with the indicated drug and dose for a period of 48 h. Densitometric analysis of the acetyl- α -tubulin to total tubulin in these HEK293 cells was performed and the resulting ratios normalized to the 10 μM dose of TubA. Graphs are depicted as mean \pm SEM of the resulting ratiometric values (test compounds: n = 3 or 4; TubA: n = 4, vehicle: n = 4). Statistical significance was analyzed by one-way ANOVA in comparison with the vehicle group. * $p < 0.05$, ** $p < 0.01$, *** $p < 0.001$. (d-f) α -Tubulin/histone acetylation assays in N2a cells. N2a cells were treated with 1 μM or 10 nM of SW-100. TubA and TSA were used as positive controls. The ratios of acetylated α -tubulin to total α -tubulin and

1
2
3 acetylated histone 3 to histone 4 were quantified by western blot. Tubulin acetylation and histone
4 acetylation were repeated and normalized to the vehicle group. Graphs represent mean \pm SEM. n
5 = 4. Statistical significance was analyzed by one-way ANOVA in comparison with the vehicle
6 group. $**p < 0.01$. n/d, not determined.
7
8
9
10
11

12 13 **Efficacy studies of HDAC6i SW100 in *Fmr1*^{-/-} mice modeling the learning and memory** 14 **deficits of FXS.** 15 16

17
18 Given its excellent potency, target selectivity, as well as its improved brain penetrance, SW-100
19 was deemed a suitable candidate for studies in animal models of CNS disorders such as the FXS
20 mouse model. We advanced SW-100 into preliminary behavioral experiments to assess if this class
21 of HDAC6i could show the potential for ameliorating learning and memory impairments in *Fmr1*^{-/-}
22 mice that display several phenotypes characteristic of FXS.^{73, 74} *Fmr1*^{-/-} mice were previously
23 shown to have learning disability and cognitive impairments in a variety of tasks including novel
24 object recognition, temporal ordering, and coordinate and categorical spatial processing.⁷⁵
25 Furthermore, these mice also exhibit elevated locomotor activity, but, this did not interfere with
26 the ability of *Fmr1*^{-/-} mice to explore the objects.⁷⁶ 20 mg/kg of SW-100 was administered twice a
27 day in order to compensate for its short metabolic half-life.
28
29
30
31
32
33
34
35
36
37
38
39
40

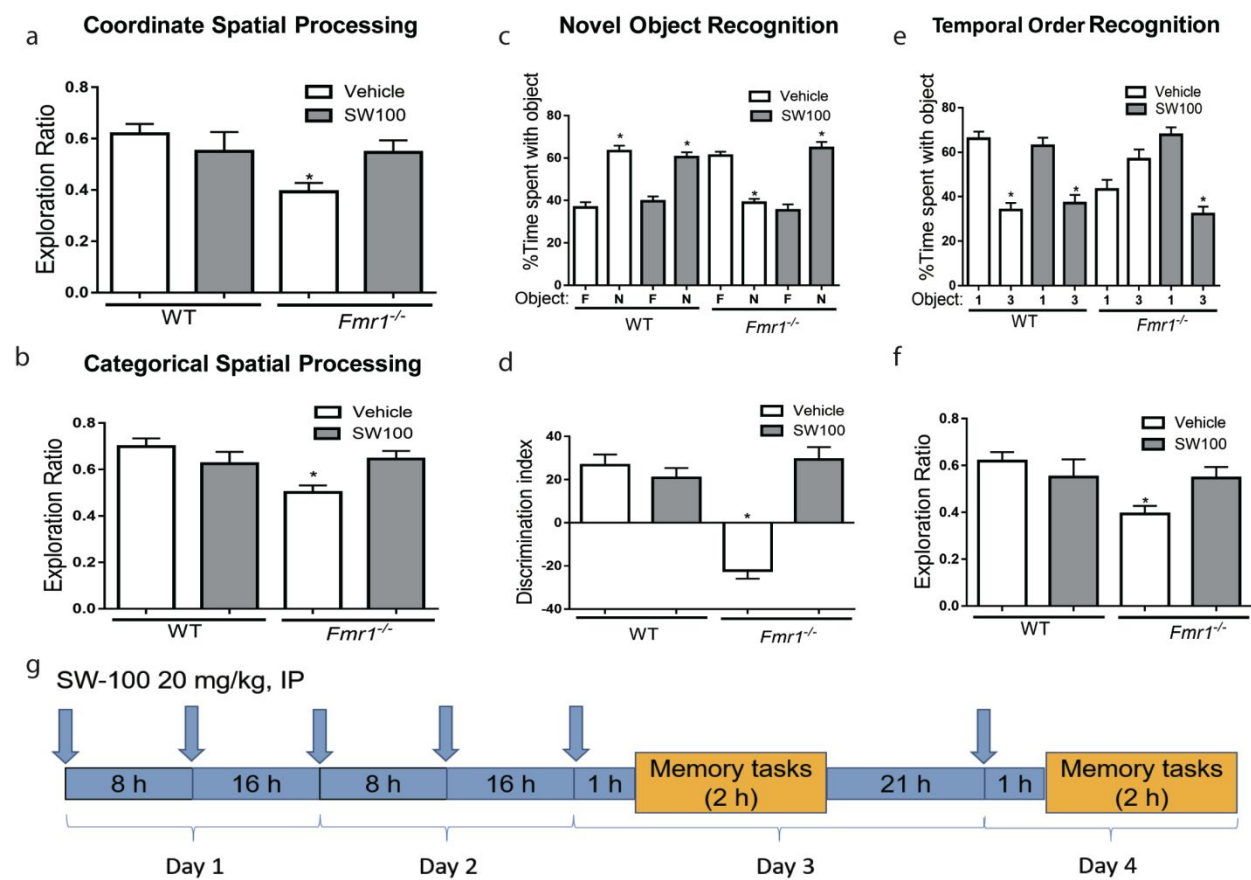
41 In the coordinate spatial processing task, the distance between two identical objects is altered
42 between the habituation and testing periods. The categorical spatial processing task involves
43 interchanging the positions of two new identical objects following the habituation phase without
44 altering the distance between them. Exploration ratios were calculated as time exploring during
45 the 5 min test session divided by time exploring during the 5 min test session plus the last 5 min
46 of the habituation session.
47
48
49
50
51
52
53
54
55
56
57
58
59
60

1
2
3 No significant differences between groups was found in total time exploring objects, when first
4 exposed to the objects, in all behavioral tests (data not shown). *Fmr1*^{-/-} mice displayed reduced
5 exploration ratios in both the coordinate [F(3,31) = 2.92, *p* < 0.05; Figure 6a] and categorical
6 [F(3,31) = 4.22, *p* < 0.05; Figure 6b] spatial processing tasks compared to WT mice. While
7 administration of SW-100 did not significantly alter the behavior of WT mice in these tests, it
8 tended to reverse the impairment in *Fmr1*^{-/-} mice in coordinate spatial processing and in categorical
9 spatial processing, so after SW-100 treatment the *Fmr1*^{-/-} mice no longer exhibited deficits
10 compared with vehicle-treated WT mice.
11
12
13
14
15
16
17
18
19
20

21 In the novel object recognition test, WT littermate mice spent significantly more time exploring
22 the novel object than the familiar object, [t(14) = 7.50, *p* < 0.01; Figure 6c]. In contrast, *Fmr1*^{-/-}
23 mice spent less time exploring the novel object, indicating that *Fmr1*^{-/-} mice do not remember the
24 familiar object [t(14) = 8.40, *p* < 0.01]. The exploration ratio (calculated by dividing the difference
25 between the time spent with the novel object *versus* the familiar object divided by total time
26 exploring) was significantly lower in *Fmr1*^{-/-} mice than WT mice [F(3,31) = 22.49, *p* < 0.01; Figure
27 6d]. Administration of SW-100 did not alter the novel object recognition of WT mice [t(16) = 6.43,
28 *p* < 0.01], but improved the abilities of *Fmr1*^{-/-} mice, which after treatment spent significantly more
29 time exploring the novel object than the familiar object [t(18) = 7.24, *p* < 0.01; Figure 6c].
30 Furthermore, the exploration ratio was significantly increased in *Fmr1*^{-/-} mice treated with SW-
31 100 [F(3,31) = 22.49, *p* < 0.01; Figure 6d], demonstrating that HDAC6 inhibition effectively
32 reversed the novel object recognition deficit in *Fmr1*^{-/-} mice.
33
34
35
36
37
38
39
40
41
42
43
44
45
46
47
48

49 WT mice displayed temporal order recognition as more time was spent exploring the initial
50 object [t(14) = 7.10, *p* < 0.01; Figure 6e], whereas *Fmr1*^{-/-} mice displayed a deficit in temporal
51 order recognition [t(14) = 2.20, *p* = 0.05; Figure 6e]. Thus, the object exploration ratio (calculated
52
53
54
55
56
57
58
59
60

by dividing the difference between the time spent with the initial object (object 1) versus the more recent object (object 3) by total time exploring), differed significantly between *Fmr1*^{-/-} and WT mice, revealing a temporal order recognition deficit in *Fmr1*^{-/-} mice [F(3,31) = 9.24, $p < 0.01$; Figure 6f]. *Fmr1*^{-/-} mice treated with SW-100 spent significantly more time exploring the first object compared to the most recent object presented, similarly to untreated or treated WT mice [WT: $t(16) = 5.00$, $p < 0.01$; *Fmr1*^{-/-} : $t(18) = 7.53$, $p < 0.01$; Figure 6e]. Furthermore, the exploration ratio was significantly increased in *Fmr1*^{-/-} mice treated with SW-100 [F(3,31) = 9.24, $p < 0.05$; Figure 6f]. These results demonstrate that temporal ordering is impaired in *Fmr1*^{-/-} mice and that this deficit is corrected by inhibition of HDAC6. Overall, we observed that *Fmr1*^{-/-} mice displayed significant deficits in these four cognitive tasks, and that administration of the HDAC6i SW-100 ameliorated all of these cognitive deficits.



1
2
3 **Figure 6.** SW-100 effects on performance of *Fmr1*^{-/-} mice in four cognitive tasks. (a) Performance
4 of WT mice (n = 17) and *Fmr1*^{-/-} mice (n = 18) in the coordinate spatial processing task (means ±
5 SEM; **p* < 0.05 compared to vehicle-treated WT mice); (b) Performance of WT mice (n = 17) and
6 *Fmr1*^{-/-} mice (n = 18) in the categorical spatial processing task (Means ± SEM; **p* < 0.05 compared
7 to vehicle-treated WT mice). (c, d) Performance of WT mice (n = 18), and *Fmr1*^{-/-} mice (n = 16)
8 in novel object recognition. (c) Percent time spent exploring the novel (N) and familiar (F) object.
9 (Means ± SEM; **p* < 0.01 compared to time spent with familiar object); (d) Discrimination index
10 (means ± SEM; **p* < 0.01 compared to vehicle-treated WT mice). (e, f) Performance of WT mice
11 (n = 17) and *Fmr1*^{-/-} mice (n = 18) on the temporal order task. (e) Percent time spent exploring the
12 first (1) and last (3) object presented. (means ± SEM; **p* < 0.05 compared to time spent with object
13 1); (f) Discrimination index (means ± SEM; **p* < 0.05 compared to vehicle-treated WT). (g)
14 Scheme of treatment and testing. Arrows indicate SW-100 treatment.

31 **α -Tubulin acetylation effects of SW-100 in the *Fmr1*^{-/-} mice.**

32
33
34 We examined the levels of acetylated α -tubulin levels in the hippocampus of the *Fmr1*^{-/-} mice
35 and WT mice. We found that the acetylated α -tubulin levels were 30% lower in the hippocampus
36 of *Fmr1*^{-/-} mice than that of WT mice [t(18) = 2.72, *p* < 0.05; Figure 7a]. The impaired acetylated
37 α -tubulin levels were significantly increased in *Fmr1*^{-/-} mice [t(16) = 4.38, *p* < 0.01; Figure 7c] by
38 treatment with SW-100, while no significant influence on hippocampal α -tubulin acetylation was
39 found in the WT mice [t(15) = 0.08 *p* = 0.93; Figure 7b]. The lack of any significant changes in
40 the acetylated α -tubulin levels in the WT mice results from the fact that estimated acetylated α -
41 tubulin levels in WT brains are approximately 75% of the total tubulin (i.e., only 25% of brain α -
42 tubulin is non-acetylated). Consequently, any putative increase (of theoretical maximum of 25%
43 to reach 100% acetylated α -tubulin) would be only marginal and difficult to quantify accurately.

To the contrary, lower basal levels of acetylated α -tubulin in *Fmr1*^{-/-} brains increase the dynamic range of the assay and allow for more accurate quantification upon inhibitor treatment.

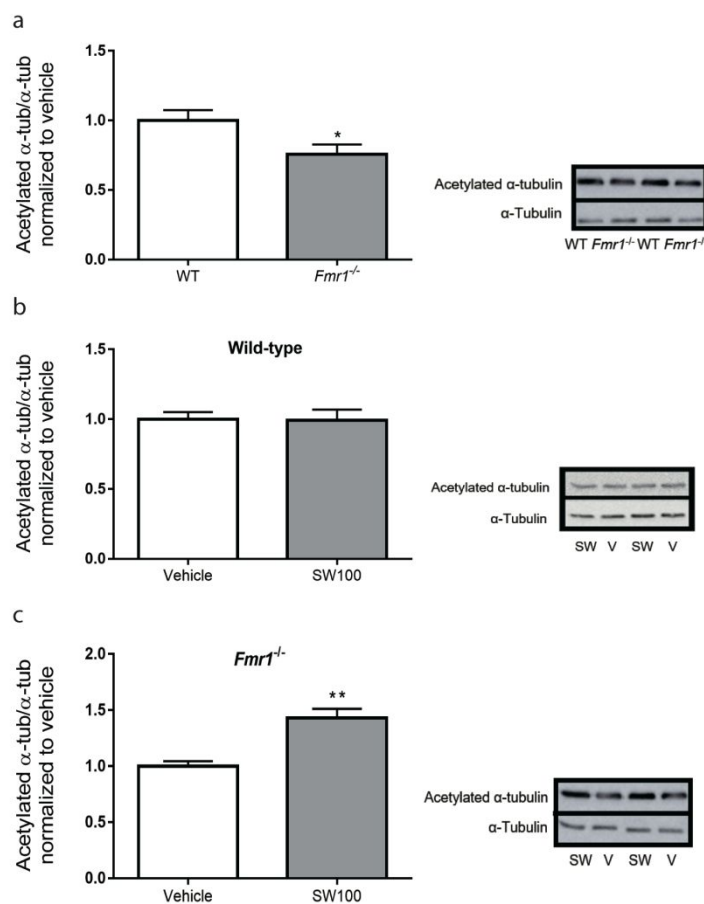


Figure 7. SW-100 electively increases the levels acetylated α -tubulin in the hippocampus of *Fmr1*^{-/-} mice. 20 mg/kg SW-100 was administered twice a day on days 1 and 2 and an additional injection was given on day 3 (1 hour prior to cognition assessments) and another injection was given on day 4 (1 hour prior to cognition assessments). (a) Basal levels of acetylated α -tubulin in the hippocampus of WT and *Fmr1*^{-/-} mice. Data were normalized relative to the WT mice. Immunoblots from representative mice in each group, at 2 h after treatment, showing acetylated α -tubulin in the hippocampus of (b) WT mice, and (c) *Fmr1*^{-/-} mice. Data were normalized to the vehicle group (0 mg/kg). Graphs represent mean \pm SEM. * p < 0.05 (a), ** p < 0.01 (c) compared to control condition. (n = 6-10 per group).

CONCLUSION

The main goal of this study was to identify a potent HDAC6 inhibitor with excellent isoform selectivity and improved BBB permeability, and then to test its ability to improve a cardinal phenotype in *Fmr1*^{-/-} mice that model intellectual deficits present in FXS patients.

In general, it would appear reasonable that a compound claimed to be selective for HDAC6 would exhibit selectivity for HDAC6 over HDAC1 in the range of 100 to a 1000-fold. However, many of the published HDAC6is exhibit relatively low selectivity *versus* other HDACs, and in particular against HDAC8 and the class IIa isozymes.⁷⁷ In contrast, the novel compound SW-100, displayed at least 1000-fold selectivity against all class I, II, and IV HDAC isoforms. These results position SW-100 as one of the most selective HDAC6is reported to date. Moreover, cellular target engagement assays revealed that SW-100 is able to displace a SAHA-based tracer from HDAC6-CD2 at low nanomolar concentrations, the key catalytic site that has been linked to the tubulin deacetylase function of HDAC6. The cellular selectivity of compound SW-100 was further investigated through α -tubulin and histone acetylation assays, and the results obtained are consistent with its HDAC isoform selectivity determined from the isolated enzyme assays.

Brain penetrance is one major challenges for the development of HDAC6is as potential therapeutics for CNS disorders due in part to the polarity of hydroxamate ZBG. Only a limited number of brain penetrable selective HDAC6is have been published in studies with animals.^{30, 33, 53, 55} While the tool compound TubA displays excellent HDAC6 selectivity, it is not particularly useful for study in animal models of CNS disorders, for as we have found it exhibits a high efflux ratio (9.83) in the MDCK-MDR1 cell line assay and thus a poor brain/plasma ratio. To overcome this weakness, we identified SW-100 that has a higher lipophilicity but lower pK_a value and thus an acceptable brain/plasma ratio.

1
2
3 Defects in α -tubulin acetylation are associated with age-related neurodegenerative diseases such
4 as Alzheimer's disease, Huntington's disease, and Parkinson's disease, amongst others.⁷⁸
5
6 Increasing the levels of acetylated α -tubulin by *Hdac6* deletion were beneficial in a mouse model
7 of ALS treatment,⁷⁹ while other articles have reported that HDAC6 inhibition in mouse models
8 of Alzheimer's disease can improve performance in various memory tasks.^{33, 54} Although the
9 exact role of α -tubulin acetylation in these diseases is still being studied, the hypothesis has
10 emerged that the defect in α -tubulin acetylation is associated with dysfunctional microtubule-
11 mediated axonal and/or dendritic transport.⁸⁰ As Fernandez-Barreda et al. stated,⁸⁰ proteins that
12 modulate the levels of microtubules are potential pharmacological targets for therapeutic strategies
13 aimed at correcting the defects in α -tubulin acetylation found in a variety of neurodegenerative
14 diseases, because alterations in α -tubulin acetylation can lead to disorganization of neuronal
15 networks.⁸¹
16
17
18
19
20
21
22
23
24
25
26
27
28
29

30 The mouse model of FXS, *Fmr1*^{-/-} mice, display cognitive impairments that can be detected in
31 measurements of novel object recognition, temporal ordering of objects, and coordinate and
32 categorical spatial processing.^{75, 82-85} Intellectual disability may be the most difficult characteristic
33 of FXS to treat, but it is critical for patients. Treatment of *Fmr1*^{-/-} mice with the HDAC6i SW-100
34 improved their performance in all four of these tasks but did not alter the performance of WT mice
35 in any of these tasks. These findings demonstrate that cognitive impairments are not irreversible
36 in this mouse model of FXS and raise the possibility that HDAC6 inhibition may be a feasible
37 therapeutic intervention for FXS.
38
39
40
41
42
43
44
45
46
47
48

49 Overall, we report the development of a new HDAC6i, SW-100, that is highly selective, potent, and
50 penetrates the CNS. *In vivo* treatment with SW-100 to *Fmr1*^{-/-} mice reversed deficits in the levels of
51 acetylated α -tubulin in the hippocampus and ameliorated several cognitive impairments. We believe
52
53
54
55
56
57
58
59
60

1
2
3 that this research offers a truly innovative approach to the treatment of FXS, and that further
4 improvements in compound design will lead to drug candidates that can be tested in humans.
5
6

7 8 **EXPERIMENTAL SECTION**

9 10 **Chemistry.**

11 12 General information.

13
14
15 ^1H and ^{13}C NMR spectra were obtained on 400/100 MHz or 300 MHz Bruker spectrometers,
16 except where noted otherwise, using the solvent residual peak as the internal reference (chemical
17 shifts: CD_3OD , 3.31/49.15; $\text{DMSO}-d_6$, 2.50/39.52; D_2O , 4.80). The following abbreviations for
18 multiplicities were used: s = singlet, d = doublet, t = triplet, q = quartet, m = multiplet, dd = double
19 doublet, dt = double triplet, td = triple doublet, ddd = double double doublet, and br s = broad
20 singlet. TLC plates (Merck silica gel 60 F_{254} , 250 μm thickness) were used to monitor reaction
21 progress, and spots were visualized under UV (254 nm). Low resolution mass spectrometry
22 (LRMS) was carried out on a Shimadzu LCMS2020-PDA+ELSD+MS, and high-resolution mass
23 spectrometry (HRMS) on a Shimadzu IT-TOF instrument under the following conditions: column,
24 ACE 3AQ (50 \times 2.1 mm i.d.); mobile phase, 8 – 100% $\text{CH}_3\text{CN}/\text{H}_2\text{O}$ containing 0.1% formic acid
25 at a flow rate of 0.5 mL/min for 4 min. Flash chromatography was performed on a Combi-Flash
26 Rf system (Teledyne ISCO) with silica gel cartridges. Preparative HPLC was performed using a
27 Shimadzu preparative LC under the following conditions: column, ACE 5AQ (150 \times 21.2 mm
28 i.d.); mobile phase: 8 – 100% MeOH (CH_3CN)/ H_2O containing 0.05% TFA at a flow rate of 17
29 mL/min for 30 min; UV detection at 254 and 280 nm. Analytical HPLC was carried out on an
30 Agilent 1260 series instrument under the following conditions: column, ACE 3 (150 \times 4.6 mm
31 i.d.); mobile phase, 8 – 100% MeOH (CH_3CN)/ H_2O containing 0.05% TFA at a flow rate of 1.0
32
33
34
35
36
37
38
39
40
41
42
43
44
45
46
47
48
49
50
51
52
53
54
55
56
57
58
59
60

1
2
3 mL/min for 25 min; UV detection at 254 nm. The purities of all tested compounds were > 98%, as
4
5 determined by analytical HPLC.

6
7
8 *4-[(Diethylamino)methyl]-N-hydroxybenzamide (2)*. (i) *General procedure A*: To KO^tBu (536.5
9
10 mg, 4.79 mmol) in anhydrous DMF (15 mL) under argon was added diethylamine (350 mg, 4.79
11
12 mmol) dissolved in anhydrous DMF (10 mL). The reaction was stirred for 15 min at 0 °C, then
13
14 methyl 4-(bromomethyl)benzoate (1.097 g, 4.79 mmol) was added as a solution in anhydrous DMF
15
16 (8 mL). The reaction was stirred for 2 h at 70 °C, and then quenched and neutralized with 2N HCl.
17
18 The residue was extracted with EtOAc (3 × 30 mL), and the combined organic layers were washed
19
20 with H₂O (2 × 30 mL) and brine (15 mL), dried over sodium sulfate, filtered, and concentrated
21
22 under vacuum. The crude product was purified *via* Combi-Flash column chromatography
23
24 (EtOAc/hexane = 0 – 100%) to afford methyl 4-[(diethylamino)methyl]benzoate as a yellow oil
25
26 (790 mg, 75%). (ii) *General Procedure B*: Solid NaOH (374 mg, 9.36 mmol) was dissolved in a 50%
27
28 aqueous solution of NH₂OH (4 mL) at 0 °C. A solution of methyl 4-
29
30 [(diethylamino)methyl]benzoate (518 mg, 2.34 mmol) in 1:1 THF/MeOH (6 mL) was added
31
32 dropwise with vigorous stirring. Upon complete addition, the ice bath was removed, and the
33
34 reaction was allowed to stir for 15 min. The reaction was then neutralized with 2N HCl solution,
35
36 and the mixture was concentrated under vacuum. The crude product was purified by preparative
37
38 HPLC to yield the title compound 2 as a white solid after neutralization and lyophilization (448
39
40 mg, 83%). ¹H NMR (400 MHz, CD₃OD) δ 7.72 and 7.42 (AA'XX' multiplet, $J_{AX} + J_{AX'} = 8.2$ Hz,
41
42 4H), 3.65 (s, 2H), 2.55 (q, $J = 7.2$ Hz, 4H), 1.08 (t, $J = 5.0$ Hz, 6H). ¹³C NMR (100 MHz, CD₃OD)
43
44 δ 166.3, 139.5, 131.9, 129.7 (2C), 127.0 (2C), 56.1, 46.4 (2C), 9.3 (2C). ESI HRMS calc. for
45
46 C₁₂H₁₉N₂O₂: [M + H]⁺, m/z 233.1441; found: 233.1441.
47
48
49
50
51
52
53
54
55
56
57
58
59
60

1
2
3 *N*-Hydroxy-4-(pyrrolidin-1-ylmethyl)benzamide (**3**). (i) The ester intermediate was synthesized
4 according to *General Procedure A* from pyrrolidine (0.12 mL, 1.52 mmol) and methyl 4-
5 (bromomethyl)benzoate (336 mg, 1.52 mmol) and isolated as a viscous clear oil (166 mg, 50%).
6
7 (ii) The title compound **3** was synthesized according to *General Procedure B* from methyl 4-
8 (pyrrolidin-1-ylmethyl)benzoate (120 mg, 0.55 mmol) and afforded as an off-white solid after
9 preparative-HPLC purification and lyophilization (38 mg, 31%). ¹H NMR (400 MHz, DMSO-*d*₆)
10 δ 11.33 (s, 1H), 10.69 (br s, 1H), 7.81 and 7.58 (AA'XX' multiplet, $J_{AX} + J_{AX'} = 8.0$ Hz, 4H), 4.39
11 (s, 2H), 3.22 (br s, 4H), 1.94 (br s, 4H). ¹³C NMR (100 MHz, CD₃OD) δ 165.6, 134.2, 133.6, 130.3
12 (2C), 127.6 (2C), 57.2, 53.6 (2C), 22.4 (2C). ESI HRMS calc. for C₁₂H₁₇N₂O₂: [M + H]⁺, *m/z*
13 221.1285; found: 221.1286.
14
15
16
17
18
19
20
21
22
23
24
25

26 *4*-(1-Pyrrolylmethyl)-*N*-hydroxybenzamide (**4**).⁶² (i) The ester intermediate was synthesized
27 from pyrrole (150 mg, 2.24 mmol) and methyl 4-(bromomethyl)benzoate (495 mg, 1.52 mmol)
28 according to *General Procedure A* and isolated as a viscous clear oil (432 mg, 90%). (ii) The title
29 compound **4** was synthesized from methyl 4-(1-pyrrolylmethyl)benzoate (400 mg, 1.86 mmol)
30 according to *General Procedure B* and afforded as a white solid after preparative-HPLC
31 purification and lyophilization (225 mg, 56%). ¹H NMR (400 MHz, CD₃OD) δ 7.69 and 7.19
32 (AA'XX' multiplet, $J_{AX} + J_{AX'} = 8.3$ Hz, 4H), 6.74 – 6.72 (m, 2H), 6.12 – 6.11 (m, 2H), 5.16 (s,
33 2H). ¹³C NMR (100 MHz, CD₃OD) δ 168.0, 144.6, 132.8, 128.5 (2C), 128.2 (2C), 122.3 (2C),
34 109.6 (2C), 53.6. ESI HRMS calc. for C₁₂H₁₃N₂O₂: [M + H]⁺, *m/z* 217.0972; found: 217.0974.
35
36
37
38
39
40
41
42
43
44
45
46

47 *4*-(1-Indolylmethyl)-*N*-hydroxybenzamide (**5**).⁶² (i) The ester intermediate was synthesized
48 according to *General Procedure A* (substituting NaH for KO^tBu) from methyl 4-
49 (bromomethyl)benzoate (978 mg, 4.27 mmol) and indole (500 mg, 4.27 mmol) and isolated as a
50 white solid (860 mg, 76%). (ii) The title compound **5** was synthesized according to *General*
51
52
53
54
55
56
57
58
59
60

1
2
3 *Procedure B* from methyl 4-(1-indolylmethyl)benzoate (840 mg, 3.17 mmol) and afforded as a
4 white solid after preparative-HPLC purification and lyophilization (443 mg, 53%). ¹H NMR (400
5 MHz, DMSO-*d*₆) δ 11.14 (s, 1H), 9.0 (br s, 1H), 7.67, 7.23 (AA'XX' multiplet, $J_{AX} + J_{AX'} = 8.1$
6 Hz, 4H), 7.56 (d, $J = 7.8$ Hz, 1H), 7.52 (d, $J = 3.1$ Hz, 1H), 7.42 (d, $J = 8.1$ Hz, 1H), 7.09 (t, $J =$
7 7.4 Hz, 1H), 7.02 (t, $J = 7.3$ Hz, 1H), 6.50 (d, $J = 3.0$ Hz, 1H), 5.48 (s, 2H). ¹³C NMR (100 MHz,
8 DMSO-*d*₆) δ 163.9, 141.4, 135.7, 129.2 (2C), 128.3, 127.1 (2C), 126.8 (2C), 121.2, 120.5, 119.2,
9 110.1, 101.1, 48.7. ESI HRMS calc. for C₁₆H₁₅N₂O₂: [M+ H]⁺, m/z 267.1128; found: 267.1137.

10
11
12
13
14
15
16
17
18
19 *4-(1-Pyrazolylmethyl)-N-hydroxybenzamide (6)*.⁶² (i) The ester intermediate was synthesized
20 according to *General Procedure A* from pyrazole (8.85 g, 0.13 mol) and methyl 4-
21 (bromomethyl)benzoate (30 g, 0.13 mol), and then isolated as a viscous yellow oil (24.5 g, 86%).
22 (ii) The title compound **6** was synthesized according to *General Procedure B* from methyl 4-(1-
23 pyrazolylmethyl)benzoate (20 g, 0.09 mmol) and afforded as a white solid after column
24 chromatography and recrystallization (11.17 g, 56%). ¹H NMR (300 MHz, DMSO-*d*₆) δ 11.19 (br
25 s, 1H), 9.09 (br s, 1H), 7.84 (d, $J = 1.8$ Hz, 1H), 7.70 and 7.24 (AA'XX' multiplet, $J_{AX} + J_{AX'} = 8.1$
26 Hz, 4H), 7.48 (d, $J = 1.2$ Hz), 6.29 (t, $J = 2.1$ Hz, 1H), 5.38 (s, 2H). ESI HRMS calc. for
27 C₁₁H₁₂N₃O₂: [M + H]⁺, m/z 218.0924. Found: 218.0917. Purity: 99.86% (254 nm), 99.45%
28 (ELSD).
29
30
31
32
33
34
35
36
37
38
39
40
41

42 *4-[4-(Dimethylamino)benzyl]-N-hydroxybenzamide (7)*.⁶² (i) To a solution of 4-
43 (dimethylamino)phenylboronic acid (12.4 g, 75.0 mmol) and methyl 4-(bromomethyl)benzoate
44 (20 g, 90 mmol) in acetonitrile/water (500/50 mL) were added Pd(PPh₃)₄ (866 mg, 0.75 mmol)
45 and K₂CO₃ (20.7 g, 150 mmol) under an argon atmosphere. The mixture was heated to reflux and
46 stirred for 6 h. Then, the mixture was diluted with H₂O (200 mL), and the organic products were
47 extracted with EtOAc (3 × 200 mL). The combined organic layers were washed with brine (200
48 mL).
49
50
51
52
53
54
55
56
57
58
59
60

mL), dried over sodium sulfate, filtered, and concentrated under vacuum. The residue was purified by flash chromatography (0 – 10% MeOH/DCM) to yield methyl 4-[4-(dimethylamino)benzyl]benzoate as an orange oil (9.6 g, 48%). (ii) The title compound **7** was synthesized according to *General Procedure B* from methyl 4-[4-(dimethylamino)benzyl]benzoate (7.6 g, 28.3 mmol) and afforded as a white solid after column chromatography and recrystallization (6.7 g, 88%). ¹H NMR (300 MHz, DMSO-*d*₆) δ 11.11 (s), 8.95 (s), 7.64, 7.25 (AA'XX' multiplet, $J_{AX} + J_{AX'} = 8.1$ Hz, 4H), 7.03, 6.65 (AA'XX' multiplet, $J_{AX} + J_{AX'} = 8.7$ Hz, 4H), 3.84 (s, 2H), 2.83 (s, 6H). ESI HRMS calc. for C₁₆H₁₉N₂O₂: [M + H]⁺, *m/z* 271.1441; found: 271.1448. Purity: 98.66% (254 nm), 99.35% (ELSD).

4-[(6-Fluoro-2-methyl-1-benzimidazolyl)methyl]-N-hydroxybenzamide (8).⁶² To a round-bottom flask charged with 4-fluoro-2-nitroacetanilide (10 g, 50.5 mmol) in MeOH (200 mL) under an atmosphere of argon was added Pd/C (10 weight%, 1.0 g). Then a hydrogen atmosphere (balloon pressure) was established by three vacuum/purge cycles. The mixture was allowed to stir at room temperature overnight, then concentrated under vacuum to approximately one-third of its volume, filtered through a plug of Celite, and concentrated. The crude aniline intermediate was taken up in 10% AcOH in DCE (200 mL), and methyl 4-formylbenzoate (8.28 g, 50.5 mmol) and NaBH(OAc)₃ (16.7 g, 75.7 mmol) were added sequentially under an argon atmosphere. The resulting suspension was allowed to stir for 24 h at room temperature. The reaction was quenched with water (100 mL), and the solution was extracted with DCM (2 × 100 mL). The combined organic layers were washed with brine, dried over sodium sulfate, and concentrated. The crude reductive amination product was taken up in toluene (200 mL), and *p*-TsOH·H₂O (950 mg, 5.0 mmol) was added. The mixture was allowed to stir under reflux for 2 h. After cooling to room temperature, saturated aqueous sodium bicarbonate solution (100 mL) was added, and the organics

1
2
3 were extracted into EtOAc (2×100 mL). The combined organic layers were washed with brine,
4
5 dried over sodium sulfate, and concentrated under vacuum. Combi-Flash column chromatography
6
7 (0–10% MeOH/DCM) afforded the ester intermediate as a light-yellow viscous oil (5.1 g, 34%
8
9 over 3 steps). (ii) The title compound **8** was synthesized according to *General Procedure B* from
10
11 the ester intermediate (1.5 g, 5.3 mmol) and afforded as an off-white powder after preparative-
12
13 HPLC purification and lyophilization (1.2 g, 80%). ^1H NMR (400 MHz, $\text{DMSO-}d_6$) δ 11.18 (s,
14
15 1H), 9.05 (s, 1H), 7.90, 7.18 (AA'XX' multiplet, $J_{\text{AX}} + J_{\text{AX}'} = 8.4$ Hz, 4H), 7.56 (dd, $J = 8.7, 4.9$
16
17 Hz, 1H), 7.40 (dd, $J = 9.2$ Hz, 2.4 Hz, 1H), 7.01 (td, $J = 10, 2.4$ Hz, 1H), 5.51 (s, 2H), 2.49 (s, 3H).
18
19 ESI HRMS calc. for $\text{C}_{16}\text{H}_{13}\text{FN}_3\text{O}_2$: $[\text{M} - \text{H}]^-$, m/z 298.0997; found: 298.0992. Purity: 98.49% (254
20
21 nm), 100% (ELSD).
22
23
24
25

26 *3-Fluoro-N-hydroxy-4-[(2-methyl-1-benzimidazolyl)methyl]benzamide (9)*.⁶² (i) The ester
27
28 intermediate was synthesized according to *General Procedure A* (substituting K_2CO_3 for KO^tBu)
29
30 from methyl 4-(bromomethyl)-3-fluorobenzoate (6 g, 24.3 mmol) and 2-methylbenzimidazole and
31
32 isolated as a viscous orange oil (5.3 g, 73%). (ii) The title compound **9** was synthesized according
33
34 to *General Procedure B* from the ester intermediate (4.0 g, 13.4 mmol) and afforded as an off-
35
36 white powder after column chromatography and recrystallization (3.0 g, 75%). ^1H NMR (400
37
38 MHz, $\text{DMSO-}d_6$) δ 11.5 (br s, 1H), 9.21 (br s, 1H), 7.85 – 7.79 (m, 2H), 7.67 – 7.60 (m, 2H), 7.58
39
40 – 7.50 (m, 2H), 7.46 (m, 1H), 5.85 (s, 2H), 2.89 (s, 3H). ESI HRMS calc. for $\text{C}_{16}\text{H}_{13}\text{FN}_3\text{O}_2$: $[\text{M} -$
41
42 $\text{H}]^-$, m/z 298.0997; found: 298.0998. Purity: 98.17% (254 nm), 100% (ELSD).
43
44
45
46

47 *4-[(6-Chloroindolin-1-yl)methyl]-N-hydroxybenzamide (10)*.⁶³ (i) The ester intermediate was
48
49 synthesized according to *General Procedure A* (substituting K_2CO_3 for KO^tBu) from methyl 4-
50
51 (bromomethyl)benzoate (34.3 g, 150 mmol) and 6-chloroindoline (23 g, 150 mmol) and isolated
52
53 as a clear oil (40 g, 89%). (ii) The title compound **10** was synthesized according to *General*
54
55
56
57
58
59
60

1
2
3 *Procedure B* from methyl 4-[(6-chloroindolin-1-yl)methyl]benzoate (20 g, 66.4 mmol) and
4
5 afforded as a white solid after column chromatography and recrystallization (6.08 g, 30%). ¹H
6
7 NMR (CD₃OD, 300 MHz) δ 7.70 and 7.46 (AA'XX' multiplet, $J_{AX} + J_{AX'} = 8.0$ Hz, 4H), 6.98 (d,
8
9 $J = 7.8$ Hz, 1H), 6.58 (dd, $J = 7.5, 1.8$ Hz, 1H), 6.44 (d, $J = 1.5$ Hz, 1H), 4.32 (s, 2H), 3.33 (t, $J =$
10
11 8.6 Hz, 2H), 2.91 (t, $J = 8.6$ Hz, 2H). ESI HRMS calc. for C₁₆H₁₆ClN₂O₂: [M + H]⁺, 303.0895;
12
13 found: 303.0892. Purity: 98.50% (254 nm), 100% (ELSD).
14
15

16
17 *4-[(6-Fluoroindolin-1-yl)methyl]-N-hydroxybenzamide (11)*.⁶³ (i) The ester intermediate was
18
19 synthesized according to *General Procedure A* (substituting K₂CO₃ for KO^tBu) from methyl 4-
20
21 (bromomethyl)benzoate (50.3 g, 220 mmol) and 6-fluoroindoline (30 g, 220 mmol) and isolated
22
23 as a clear oil (23 g, 37%). (ii) The title compound **11** was synthesized according to *General*
24
25 *Procedure B* from methyl 4-[(6-fluoroindolin-1-yl)methyl]benzoate (11 g, 38.6 mmol) and
26
27 afforded as a white solid after column chromatography and recrystallization (6.46 g, 59%). ¹H
28
29 NMR (DMSO-*d*₆, 300 MHz) δ 11.18 (s, 1H), 9.01 (s, 1H), 7.73 and 7.40 (AA'XX' multiplet, J_{AX}
30
31 + $J_{AX'} = 8.4$ Hz, 4H), 7.00 (m, 1H), 6.40 (dd, $J = 10.8, 2.1$ Hz, 1H), 6.29 (td, $J = 8.4, 2.4$ Hz, 1H),
32
33 4.38 (s, 2H), 3.35 (t, $J = 8.2$ Hz, 2H), 2.87 (t, $J = 8.2$ Hz, 2H). ESI HRMS calc. for C₁₆H₁₆FN₂O₂
34
35 [M + H]⁺: 287.1190; found: 287.1197. Purity: 99.44% (254 nm), 100% (ELSD).
36
37
38
39

40
41 *N-Hydroxy-4-[[[(1-methyl-1H-benz[d]imidazol-2-yl)amino]methyl]benzamide (12)*.⁶³ (i) A
42
43 mixture of 1-methyl-1H-benz[d]imidazol-2-amine (1.2 g, 8.2 mmol) and methyl 4-formylbenzoate
44
45 (1.3 g, 8.2 mmol) in toluene (40 mL) was refluxed for 6 h. The excess solvent was removed, and
46
47 the residue was redissolved in a mixture of MeOH (10 mL) and THF (10 mL). Then sodium
48
49 borohydride (0.47 g, 12.2 mmol) was added at 0 °C. After stirring for 30 min, the reaction was
50
51 quenched with ice water and extracted with EtOAc (2 × 30 mL). Combined organic layers were
52
53 washed with brine, dried over Na₂SO₄, and concentrated under vacuum. The crude ester
54
55
56
57
58
59
60

1
2
3 intermediate, a yellow oil (1.5 g, 62%), was used in next step without further purification. (ii) The
4 title compound **12** was synthesized according to *General Procedure B* from methyl 4-[[1-methyl-
5 1*H*-benz[*d*]imidazol-2-yl)amino]methylbenzoate (1.5 g, 5.1 mmol) and afforded as a white solid
6 after column chromatography and recrystallization (800 mg, 53%). ¹H NMR (D₂O, 300 MHz) δ
7 7.65 and 7.46 (AA'XX' multiplet, $J_{AX} + J_{AX'} = 8.3$ Hz, 4H), 6.92 (m, 2H), 4.71 (s, 2H), 3.59 (s,
8 3H). ESI HRMS calc. for C₁₆H₁₇N₄O₃ [M + H]⁺: 297.1346; found: 297.1352. Purity: 99.30% (254
9 nm), 100% (ELSD).

10
11
12
13
14
15
16
17
18
19
20
21
22
23
24
25
26
27
28
29
30
31
32
33
34
35
36
37
38
39
40
41
42
43
44
45
46
47
48
49
50
51
52
53
54
55
56
57
58
59
60
3-Chloro-N-(4-chlorophenyl)propanamide (14). To a round bottom flask charged with 4-
chloroaniline (**13**, 5.0 g, 39.37 mmol) in acetone (50 mL) was added 3-chloropropanoyl chloride
(1.9 mL, 19.69 mmol) at room temperature. The resulting mixture was allowed to stir for 1 h under
reflux condition. Then the reaction was cooled to room temperature and quenched with 2N HCl
(30 mL), and then extracted with EtOAc (3 × 25 mL). The combined organic extracts were washed
with brine (20 mL), dried over Na₂SO₄, and concentrated under vacuum. The crude product was
used directly without further purification, and the title compound **14** was obtained as off-white
powder (4.6 g, 54%). ¹H NMR (CDCl₃) δ 7.56 (br s, 1H), 7.46 (d, $J = 8.7$ Hz, 2H), 7.28 (d, $J = 8.8$
Hz, 2H), 3.87 (t, $J = 6.3$ Hz, 2H), 2.81 (t, $J = 6.3$ Hz, 2H). ¹³C NMR (CDCl₃) δ 167.9, 136.0, 129.8,
129.1 (2C), 121.4 (2C), 40.4, 39.8.

6-Chloro-1,2,3,4-tetrahydroquinoline (15). (i) In a three-necked flask charged with **14** (4.6 g,
21.1 mmol) under an argon atmosphere was added AlCl₃ (5.47 g, 42.2 mmol) at 140 °C. The
resulting mixture was stirring at the same temperature for 12 h. Then the reaction was quenched
with 1 N HCl (20 mL) carefully at 0 °C and extracted with EtOAc (3 × 30 mL). The combined
organic extracts were washed with brine (20 mL), dried over Na₂SO₄, and concentrated under
vacuum. The crude product was purified by flash chromatography (0 – 80% EtOAc/Hexane) to

1
2
3 afford as white powder (3.1 g, 17.1 mmol). (ii) To a stirred solution of LiAlH₄ (1.952 g, 51.4 mmol)
4 in THF (30 mL) were dropwise added lactam intermediate (3.1 g, 17.1 mmol) in THF (20 mL) at
5
6 0 °C. The resulting mixture was stirred at same temperature for 20 min, then heated at reflux
7
8 condition for additional 1 h. The reaction was subsequently quenched with water (2.0 mL), 5 N
9
10 NaOH (2.0 mL), and water (10 mL). The afforded precipitate was filtered off and washed with
11
12 EtOAc (3 × 20 mL). The filtrate was washed with brine (20 mL), dried over Na₂SO₄, and
13
14 concentrated under vacuum. The product **6a** was obtained as colorless oil (2.43 g, 69.5% for two
15
16 steps) and used directly into next step without further purification. ¹H NMR (CDCl₃) δ 6.93 – 6.86
17
18 (m, 2H), 6.38 (d, *J* = 8.0 Hz, 1H), 3.77 (br s, 1H), 3.33 – 3.15 (m, 2H), 2.72 (t, *J* = 6.4 Hz, 2H),
19
20 1.94 – 1.88 (m, 2H). ¹³C NMR (CDCl₃) δ 143.2, 128.8, 126.3, 122.7, 120.9, 114.9, 41.7, 26.7, 21.6.
21
22
23
24
25

26 *4-((6-Chloro-3,4-dihydroquinolin-1(2H)-yl)methyl)-N-hydroxybenzamide (SW-100)*. (i) To a
27
28 round bottom flask charged with 6-chloro-1,2,3,4-tetrahydroquinoline (**15**, 2.43 g, 14.6 mmol) and
29
30 methyl 4-(bromomethyl)benzoate (4.99 g, 21.9 mmol) in DMF (30 mL) was added K₂CO₃ (4.03
31
32 g, 29.2 mmol). The resulting mixture was allowed to stir at 100 °C for 2 h. After completion of the
33
34 reaction, the solution was cooled to room temperature, quenched with H₂O (30 mL), and extracted
35
36 with EtOAc (3 × 20 mL). The combined organic extracts were washed with brine (20 mL), dried
37
38 over Na₂SO₄, and concentrated under vacuum. The crude product was purified by flash
39
40 chromatography (0 – 20% EtOAc/Hexane) to afford ester intermediate as white solid (3.6 g, 78%).
41
42 (ii) The title compound SW-100 was synthesized according to *General Procedure B* from methyl
43
44 4-((6-chloro-3,4-dihydroquinolin-1(2H)-yl)methyl)benzoate (3.6 g, 11.4 mmol) and afforded as a
45
46 white solid (1.8 g, 50%) after preparative-HPLC purification and lyophilization. ¹H NMR (DMSO-
47
48 *d*₆) δ 11.16 (s, 1H), 8.94 (br s, 1H), 7.70 (AA'XX' multiplet, *J*_{AX} + *J*_{AX'} = 8.2 Hz, 2H), 7.28
49
50 (AA'XX' multiplet, *J*_{AX} + *J*_{AX'} = 8.1 Hz, 2H), 6.94 (d, *J* = 2.4 Hz, 1H), 6.87 (dd, *J* = 8.8, 2.5 Hz,
51
52
53
54
55
56
57
58
59
60

1
2
3 1H), 6.36 (d, $J = 8.8$ Hz, 1H), 4.51 (s, 2H), 3.39 – 3.35 (m, 3H), 2.73 (t, $J = 6.1$ Hz, 2H), 1.96 –
4
5 1.82 (m, 2H). ^{13}C NMR (DMSO- d_6) δ 164.2, 143.7, 142.0, 131.4, 128.2, 127.2 (2C), 126.5 (2C),
6
7 126.4, 123.9, 118.7, 111.9, 53.9, 27.4, 21.4. ESI HRMS calcd. for $\text{C}_{17}\text{H}_{16}\text{ClN}_2\text{O}_2$: $[\text{M}-\text{H}]^-$, m/z
8
9 316.0906; found: 316.0899. Purity: 99.39% (254 nm), 100% (ELSD).

12 **Docking simulation.**

14 The crystallographic structure of HDAC6 were obtained from the Protein Data Bank (PDB) with
15 the access code 5G0I (resolution of 1.99 Å).⁸⁶ The three-dimensional (3D) structures of
16
17 compounds **1-5**, **16**, SW100, and TubA were built up in their neutral forms by molecular mechanics
18
19 using Merck molecular force field (MMFF94) using Spartan'14 software (Wavefunction, Inc.). The
20
21 equilibrium geometry at ground state were calculated with the Density Functional Theory (DFT),
22
23 method Becke, three-parameter, Lee-Yang-Parr (B3LYP) with the standard 6-31G* basis set
24
25 available in Spartan'14. All docking simulations were performed with the GOLD 5.4 software
26
27 (CCDC), in the catalytic domain 2 (CD2) of HDAC6. GOLD 5.4 has four fitness functions
28
29 available: GoldScore, ChemScore, ASP, and ChemPLP. All fitness functions were evaluated by
30
31 re-docking of the co-crystallized ligand to identify the most suitable fitness function for the
32
33 docking into HDAC6. Crystallographic waters were removed during the docking runs. Hydrogen
34
35 atoms were added to the protein according to the data inferred by the program on the ionization
36
37 and tautomeric states. The set of amino acid residues selected as the binding cavity was delimited
38
39 by a 10 Å radius from the co-crystallized ligand. The Zn^{2+} ion was maintained at the catalytic site
40
41 in order to evaluate its coordination with each ligand. After re-docking, the root-mean-square
42
43 deviation (RMSD) between the best result for each fitness function, and the experimental
44
45 conformation of each co-crystallized ligands were calculated. The fitness function with the lower
46
47 value of RMSD (< 2.0 Å), and the best performance in the re-docking was used for the docking of
48
49
50
51
52
53
54
55
56
57
58
59
60

1
2
3 compounds **1-5**, **16**, SW-100, and TubA. ChemPLP was the best fitness function found (higher
4
5 RMSD obtained equal to 0.357 Å). The number of genetic operations (crossover, migration,
6
7 mutation) in each docking run used in the searching procedure was set to 100,000. The program
8
9 optimizes hydrogen-bond geometries by rotating hydroxyl and amino groups of the amino acid
10
11 side chains. The score of each pose identified is calculated as the negative of the sum of a series
12
13 of energy terms involved in the protein-ligand interaction process, thus the more positive the score
14
15 is, the better the interaction. The interaction between **1** and HDAC6-CD2 was obtained from PDB
16
17 with the access code 6CSR.⁶¹
18
19

20 21 **HDAC1-11 enzyme assays.** 22

23
24 HDAC inhibition assays were performed by the Reaction Biology Corporation (Malvern, PA)
25
26 using human full-length recombinant HDAC1-11 isoforms. Compounds **6-12**, SW-100, TubA, and
27
28 NexA were tested in duplicate 10-dose IC₅₀ mode with 3-fold serial dilution starting at 30 μM
29
30 against all HDAC isoforms. Trichostatin A (TSA) and TMP269 were tested as references in a 10-
31
32 dose IC₅₀ with 3-fold serial dilution starting at 10 μM. A fluorogenic peptide derived from residues
33
34 379-382 of p53 (RHKK(Ac)AMC) was used as the substrate for HDAC1, 2, 3, 6, 10, and 11; a
35
36 fluorogenic peptide containing a trifluoroacetylated lysine, Ac-LGK(TFA)-AMC, was used as the
37
38 substrate for HDAC4, 5, 7, and 9; and a fluorogenic peptide derived from p53 residues 379-382
39
40 (RHK(Ac)K(Ac)AMC) was used as the substrate for HDAC8. IC₅₀ values were calculated using
41
42 the GraphPad Prism 4 program based on a sigmoidal dose-response equation. The blank (DMSO)
43
44 value was entered as 1.0×10^{-12} of concentration for curve-fitting. The reaction buffer contained:
45
46 50 mM Tris·HCl pH 8.0, 137 mM NaCl, 2.7 mM KCl, 1 mM MgCl₂, 1 mg/mL BSA, and a final
47
48 concentration of 1% DMSO. The enzyme was added into wells of the reaction plate, and stock
49
50 solutions of compounds were distributed into the enzyme mixture by acoustic technology
51
52
53
54
55
56
57
58
59
60

(Echo550 instrument; nanoliter range). The plates were spun down and pre-incubated for 5-10 min. The substrate was then delivered to all reaction wells to initiate the reaction, which was incubated for 2 h at 30 °C. After incubation, developer and tested compound were added to quench the reaction and generate fluorescence. Kinetic measurements were then taken for 1.5 h at 15 min intervals to ensure that development was complete. Endpoint readings were taken for analysis after the development reached a plateau.

HDAC6 and 11 data of SW100 were repeated and confirmed in Dr. Cyril Bařinka's lab.

Permeability studies in MDCK-MDR1 cells.

Permeability studies were performed by Pharmaron, Inc (Irvine, CA). MDCK-MDR1 cells were cultured in DMEM medium supplemented with 20% FBS and maintained at 37 °C and 5% CO₂. Cell monolayers were prepared by culturing MDCK-MDR1 cells in 96-well HTS transwell plates at a starting cell density of 1 × 10⁵ cells/m² for 4-8 days. Integrity of the monolayer was confirmed by measuring TEER (transepithelial electric resistance) and TEER value > 300 Ω*cm² were used for assay. Test compounds were added into the donor chambers (both apical and basolateral), and the transwell plates were incubated at 37 °C for 2 h. Transwells were separated, and samples from donor and receiver chambers were collected. Compound concentrations were determined by LC-MS/MS (LC system: Shimadzu; MS analysis: API 4000). Apparent permeability (P_{app}) was calculated according to the equation:

$$P_{app} = (VA / (\text{Area} \times \text{time})) \times ([\text{drug}]_{\text{receiver}} / ([[\text{drug}]_{\text{initial, donor}}] \times \text{Dilution Factor})),$$

where VA is the volume in the acceptor well.

Pilot brain and plasma pharmacokinetic studies.

Pharmacokinetics (PK) studies were performed by Pharmaron, Inc (Irvine, CA). To generate a stock solution, 4.14 mg of compound SW-100 was dissolved in 0.104 mL DMSO. Then 0.414 mL

1
2
3 of PEG-400 and 0.518 mL of saline were added to this solution with vortexing to obtain a final
4 volume of 1.036 mL. The final concentration of the formulation solution (10% DMSO:40%
5 PEG400:50% saline) was 4 mg/mL. According to our previous experience with TubA,^{31,35} a drug
6 dosage of 20 mg/kg was administered into C57BL/6 male mice *via* a single intraperitoneal (IP)
7 injection.
8
9

10
11
12
13
14
15 Approximately 0.025 mL blood was collected from 2 mice/group at two points (60 and 240 min)
16 after injection. All blood samples were transferred into plastic micro centrifuge tubes containing
17 heparin-Na as anti-coagulant. Collection tubes with blood samples and anticoagulant were inverted
18 several times for proper mixing of the tube contents and then placed on wet ice prior to
19 centrifugation for plasma. Blood samples were centrifuged at $4,000 \times g$ for 5 min at 4 °C to obtain
20 plasma. Mice were sacrificed to collect brain samples from other two groups (2 mice/group) at two
21 points (60 and 240 min) after injection. Brain tissues were weighed accurately and were
22 homogenized at a 1:4 ratio of tissue weight (g) to volume of PBS (mL). The data found (ng/mL)
23 was multiplied with five to obtain concentration (ng/mL) in brain tissues. Plasma samples and
24 brain homogenates were stored below -70 °C until analysis. 30 μ L Plasma samples or brain
25 homogenate were diluted with 3 μ L of blank matrix, and then 200 μ L of acetonitrile containing
26 internal standard was added for precipitating protein. The mixture was vortexed for 2 min and
27 centrifuged at $4,000 \times g$ for 15 min at 4 °C. 10 μ L of the supernatant after diluting 3 times with
28 water was taken for LC-MS/MS analysis (LC system: Shimadzu; MS analysis: API 4000). All
29 samples were processed on ice.
30
31
32
33
34
35
36
37
38
39
40
41
42
43
44
45
46
47
48

49 **α -Tubulin acetylation studies in HEK293 cells.**

50
51
52 HEK293 cells were grown in DMEM containing 4.5 g/L D-glucose, L-glutamine, 1mg/L sodium
53 pyruvate, supplemented with 10% FBS and 1% penicillin/streptomycin. 24 h prior to treatment,
54
55
56
57
58
59
60

1
2
3 cells were plated on twelve-well plates. Once 70% confluency was reached, the media was
4
5 aspirated and replaced with media containing HDAC6i at concentrations of 10 nM, 100 nM, 1 μ M
6
7 and 10 μ M. Cells were treated for 24 h, then were washed with DPBS and harvested. Cells were
8
9 lysed in Mammalian Protein Extraction Reagent (MPER) lysis buffer with added protease
10
11 inhibitors, and protein concentrations determined for the lysates using the DC Protein
12
13 Concentration Assay. Loading buffer was added to 2 μ g of protein, and samples were incubated
14
15 in a boiling water bath for 5 min to ensure denaturation. Electrophoresis of these samples was
16
17 performed on 5% stacking and 12% resolving polyacrylamide gels in Tris-glycine running buffer
18
19 (25 mM Tris-base, 192 mM glycine, 0.1% SDS), and then electro-transferred to a PVDF
20
21 membrane in transfer buffer (25 mM Tris-base, 192 mM glycine, 20% methanol) overnight at 4
22
23 $^{\circ}$ C. The membranes were then blocked in 5% skim milk powder dissolved in TBST (10 mM Tris,
24
25 150 mM NaCl, 0.05% Tween) for 2 h at room temperature, then treated with mouse anti-acetyl-
26
27 tubulin primary antibody at a 1:3000 dilution in blocking solution overnight at 4 $^{\circ}$ C. The
28
29 membranes were washed thoroughly in TBST, then probed with HRP-tagged goat anti-mouse
30
31 secondary antibody, diluted in blocking solution (1:5000) for 2 h at room temperature. Upon
32
33 further washing in TBST, membranes were treated with ECL detection reagents, then developed
34
35 on film. To account for total cellular α -tubulin in addition to protein loads, the membrane was
36
37 stripped and re-probed with rabbit anti- α -tubulin primary (1:1000) and goat anti-rabbit (1:5000)
38
39 secondary antibodies in a similar fashion. Signal was assessed through densitometry using ImageJ
40
41 software.
42
43
44
45
46
47
48

49 **Cell transfection, treatments, and BRET measurements.**

50
51 NanoBRET target engagement was performed against HDAC6 (CD2) and HDAC1 according to
52
53 the manufacturer's protocol (Promega) in HEK293 cells (ATCC). Plasmid constructs encoding
54
55
56
57
58
59
60

1
2
3 NanoLuc-HDAC6 (CD2) and HDAC1-NanoLuc encoded HDAC open reading frames matching
4 previous work.⁶⁵ HDAC6 (CD2) encoded a GSSGAIA linker between Nanoluc and HDAC6
5
6 (CD2) and HDAC1-NanoLuc encoded a SWTWEGNKWTWK linker between HDAC1 and
7
8 NanoLuc. For target engagement analysis for HDAC6, a HEK293 cell line stably expressing full-
9
10 length NanoLuc-HDAC6 was used (Promega). NanoBRET HDAC Tracer (Promega) was added
11
12 to a final concentration of 250 nM, 1000 nM, or 100 nM for HDAC6 (CD2), HDAC1, and HDAC6
13
14 (respectively) immediately prior to test compound addition. Tracer concentrations were selected
15
16 for each HDAC such that tracer occupancy did not impart a shift in observed compound IC₅₀ value.
17
18
19 Serially-diluted test compounds were then added to the cells and allowed to equilibrate for 2 h
20
21 prior to BRET measurements. To measure BRET, NanoBRET NanoGlo Substrate-(Promega) and
22
23 Extracellular NanoLuc inhibitor was added per the manufacturer's protocol, and filtered
24
25 luminescence was measure on GloMax Discover luminometer equipped with 450 nm BP filter
26
27 (donor) and 610 nm LP filter (acceptor), using 0.5 s integration time. Milli-BRET units (mBU) are
28
29 the BRET values × 1000. Competitive displacement data were then graphed with GraphPad Prism
30
31 software using a three-parameter curve-fitting with the following equation:
32
33
34
35
36
37

$$Y = \text{Bottom} + (\text{Top} - \text{Bottom}) / (1 + 10^{((X - \text{LogIC}_{50}))})$$

38 **α-Tubulin/histone acetylation studies in N2a cells.**

39
40
41
42 Cells were washed with phosphate-buffered saline (PBS) and collected using the EpiQuik Total
43
44 Histone Extraction Kit (EpiGentek). Protein concentrations were determined using the micro BCA
45
46 kit (ThermoFisher Scientific) according to manufacturer's protocol. Protein samples were
47
48 supplemented with reducing sample buffer (Thermo Scientific) and denaturized by incubating at
49
50 95 °C for 5 min. The nonspecific binding was blocked by incubation of the PVDF membrane in
51
52 5% bovine serum albumin (BSA), diluted in Tris Buffered Saline Tween (TBST, 50 mM TRIS,
53
54
55
56
57
58
59
60

1
2
3 150 mM NaCl, 0.1% Tween-20 (Appllichem) for 1 h at room temperature followed by incubation
4
5 with primary antibodies overnight. The antibodies, diluted in TBST, were directed against
6
7 α -tubulin (1:5000, T6199, Sigma-Aldrich), acetylated α -tubulin (1:5000, T6793 monoclonal,
8
9 Sigma-Aldrich), histone H3 acetyl k9+k14 (1:1000, 9677L, Cell Signaling), and histone 4 (1:1000,
10
11 ab10158, Abcam). Secondary antibodies conjugated with horseradish peroxidase (Dako, 1:5000,
12
13 1h, RT) were used prior to detection with ECL substrate (life technologies) with a LAS 4000
14
15 Image Analyser (GE Healthcare). Luminescent signals were quantified with ImageQuant TL 7.0
16
17 software (GE Healthcare) and then graphed with GraphPad Prism software. A mild reblotting
18
19 buffer (Merck Millipore Corp.) was applied to strip the blots.
20
21
22
23

24 **Behavior amelioration study in *Fmr1*^{-/-} mice.**

25
26 Male adult (8-10 weeks old) C57BL/6 WT mice, and C57BL/6 mice with a disruption of the
27
28 *Fmr1* gene (originally kindly provided with matched controls by Dr. W. Greenough, University of
29
30 Illinois) were used. Mice were housed in groups of 3-5 in standard cages in light and temperature-
31
32 controlled rooms and were treated in accordance with NIH and the University of Miami
33
34 Institutional Animal Care and Use Committee regulations. Mice were treated with drugs through
35
36 IP administration twice a day (20 mg/kg) for two days and 1 hour prior to cognition testing on the
37
38 3rd and 4th days.
39
40
41

42 Four cognitive tasks were tested: coordinate and categorical spatial processing, novel object
43
44 recognition, and temporal order memory, carried out as previously described.^{75, 85, 87} Mice were
45
46 habituated to the testing room with a white noise generator (55 dB) for 1 hour. Behavioral tests
47
48 were conducted during 2 consecutive days, two tests every 24 hours (shown in Figure 6g). 70%
49
50 ethanol was used to clean each apparatus and object used between each test session. Test sessions
51
52 were filmed, and films were scored by an investigator blind to the genotype and treatment. Mice
53
54
55
56
57
58
59
60

1
2
3 were assessed in the novel object recognition task and coordinate spatial processing task on Day 3
4
5 and were assessed in the temporal ordering task and categorical spatial processing task on Day 4.
6
7

8 For the coordinate spatial processing task, each mouse was allowed to explore two novel objects
9
10 that were 45 cm apart for 15 min. After 5 min in an opaque chamber, each mouse was allowed to
11
12 explore the same two objects that had been moved closer together (30 cm) for 5 min. Increased
13
14 exploration of the objects during the test session compared with the last 5 min of the habituation
15
16 phase was considered a measure of memory of the distance between objects. The exploration ratio
17
18 was calculated as time (exploring during the 5 min test session)/(exploring during the 5 min test
19
20 session plus the last 5 min of the habituation session).
21
22
23

24 For the categorical spatial processing task, each mouse was allowed to explore two novel objects
25
26 that are 45 cm apart for 15 min. After 5 min in an opaque chamber, each mouse was allowed to
27
28 explore the same two objects that had been transposed for 5 min. Increased exploration of the
29
30 objects during the test session compared with the last 5 min of the habituation phase is considered
31
32 a measure of memory of the distance between objects. The exploration ratio was calculated as time
33
34 (exploring during the 5 min test session)/(exploring during the 5 min test session plus the last 5
35
36 min of the habituation session).
37
38
39

40 For the novel object recognition task, time spent exploring an object only includes the mouse
41
42 sniffing or touching the object with its nose, vibrissa, mouth, or forepaws. As described
43
44 previously,⁸⁷ novel object recognition was measured by allowing each mouse to explore two
45
46 identical objects for 5 min, and after a 5 min period in an opaque chamber, mice were allowed to
47
48 explore an unused familiar object and a novel object for 5 min. The discrimination index was
49
50 calculated as the times ((exploring object 2 – exploring object 1)/total time of object exploration)
51
52 × 100). To measure temporal order memory, each mouse underwent three sessions exploring three
53
54
55
56
57
58
59
60

1
2
3 new sets of objects (objects 1, 2, 3). During the test session, the mouse was allowed to explore an
4 unused copy of object 1 and an unused copy of object 3 for 5 min. Intact temporal order memory
5 was evident when mice spent more time exploring the first object presented (object 1) than the
6 most recent object presented (object 3). A discrimination index was calculated as the times
7
8
9
10
11
12 ((exploring object 3 – exploring object 1)/total time of object exploration) × 100).
13

14 **Immunoblot analysis of mice samples.**

15
16
17 Mouse hippocampi were rapidly dissected in ice-cold phosphate-buffered saline and
18 homogenized in ice-cold lysis buffer containing 20 mM Tris-HCl, pH 7.4, 150 mM NaCl, 2 mM
19 EDTA, 1% Triton X-100, 10% glycerol, 1 µg/mL leupeptin, 1 µg/mL aprotinin, 1 µg/mL pepstatin,
20
21
22 1 mM phenylmethanesulfonyl fluoride, 50 mM NaF, 1 mM sodium orthovanadate, and 100 nM
23 okadaic acid. The lysates were centrifuged at $20,800 \times g$ (14,000 rpm) for 10 min. Protein
24 concentrations in the supernatants were determined using the Bradford protein assay.⁸⁸ Lysates
25 were mixed with Laemmli sample buffer (2% SDS) and placed in a boiling water bath for 5 min.
26
27
28 Proteins (10 µg) were resolved in SDS-polyacrylamide gels, transferred to nitrocellulose, and
29 incubated with primary antibodies to acetylated α -tubulin (1:4000, T7451, Sigma Aldrich) or α -
30 tubulin (1:4000, T5168, Sigma Aldrich). Double loading was used to measure ratio for each
31 protein. Immunoblots were developed using horseradish peroxidase-conjugated goat anti-mouse,
32 followed by detection with enhanced chemiluminescence.
33
34
35
36
37
38
39
40
41
42
43

44 **Statistical analysis.**

45
46
47 Statistical significance was assessed by one-way ANOVA or by Student's t-test when indicated.
48
49 GraphPad Prism 6 or 7 software was used. All data were expressed as mean \pm SEM, and
50 significance was set at $p < 0.05$.
51
52

53 **ASSOCIATED CONTENT**

Supporting Information Available:

The supporting information contains additional tables, figures, and, ^1H and ^{13}C -NMR spectra and purity reports for compounds **6-12**, SW-100, TubA, and NexA. This material is available free of charge via the Internet at <http://pubs.acs.org>.

AUTHOR INFORMATION**Corresponding Author Information**

*A.P.K.: E-mail: akozikowski@starwisetrx.com; Phone: (+1)773 793 5866

ORCID

Alan P. Kozikowski: 0000-0003-4795-5368

Sida Shen: 0000-0002-0295-2545

Marta Pardo: 0000-0003-0808-1303

Maurício T. Tavares: 0000-0002-4400-7787

Present Addresses

†Current address:

S.S.: Departments of Chemistry and Molecular Biosciences, Chemistry of Life Processes Institute, Center for Molecular Innovation and Drug Discovery, and Center for Developmental Therapeutics, Northwestern University, Evanston, Illinois 60208, United States

M.P.: Department of Neurology, Miller School of Medicine, University of Miami, Miami, FL 33136, United States

1
2
3 M.T.T: Faculty of Pharmaceutical Sciences, Department of Pharmacy, University of São Paulo,
4
5 São Paulo, Brazil.
6
7

8 **Author Contributions**

9

10
11 ‡S.S. and M.P. contributed equally to this paper.
12
13

14 StarWise Therapeutics LLC: A.P.K. conceived the original idea, initiated the project, and oversaw
15 all the experimental design and data analysis. University of Illinois at Chicago: S.S. designed and
16 synthesized compounds, oversaw all the experimental design, analyzed data, and wrote the
17 manuscript with assistance from the other authors; M.T.T. synthesized compounds, performed the
18 docking studies, and assisted in the preparation of the manuscript; G.Z synthesized some of the
19 reported compounds. University of Miami: M.P. designed and performed the *in vivo* FXS mice
20 model studies and assisted in the preparation of the manuscript, R.S.J. oversaw the experimental
21 design and data analyses of animal studies. University Health Network: D.S. designed and
22 performed the dose-response tubulin acetylation studies in HEK293 cells and assisted in the
23 preparation of the manuscript and J.H.E. oversaw the experimental design and data analyses of the
24 *in vitro* tubulin acetylation study. Leuven Research Institute for Neuroscience and Disease: V.B.
25 designed and performed the tubulin/histone acetylation studies in N2a and assisted in the
26 preparation of the manuscript; L.V.D.B. oversaw the experimental design and data analyses of the
27 *in vitro* tubulin acetylation study. Promega Corporation: C.A.Z. designed and performed the
28 cellular HDAC target engagement assay; M.B.R. oversaw the experimental design and data
29 analyses of target engagement study and assisted in the preparation of the manuscript. Institute of
30 Biotechnology of the Czech Academy of Sciences: Z.K. performed and confirmed the HDAC6
31 and HDAC11 data for SW-100. C.B. oversaw the experimental design and data analyses of HDAC
32 enzyme studies.
33
34
35
36
37
38
39
40
41
42
43
44
45
46
47
48
49
50
51
52
53
54
55
56
57
58
59
60

Notes

Dr. Kozikowski is the owner of StarWise Therapeutics LLC and thus declares potential financial interests as does Dr. Zhang who is employed by StarWise Therapeutics.

ACKNOWLEDGMENTS

The authors thank B. Havlinova for excellent technical assistance. This work was supported by grants from the NIH (NS079183, to A.P.K. and L.V.D.B) and the CIHR (PJT-153015; to J.H.E), and a NARSAD Distinguished Investigator Grant to R.S.J. from the Brain & Behavior Research Foundation. This work was also in part supported by the Czech Science Foundation (15-19640S), the CAS (RVO: 86652036), and the project “BIOCEV” (CZ.1.05/1.1.00/02.0109) from the ERDF.

ABBREVIATIONS

ADMET, absorption, distribution, metabolism, excretion, and toxicity; GSK-3 β , glycogen synthase kinase-3beta; ERK1/2, extracellular signal-regulated kinase 1 and 2; IGF1, insulin-like growth factor 1; MMP9, matrix metalloproteinase 9; SIRT, sirtuins; DMF, *N,N*-dimethylformamide; DMSO, dimethyl sulfoxide; DCM, dichloromethane; DCE, 1,2-dichloroethene; THF, tetrahydrofuran; TLC, thin layer chromatography; HPLC, high performance liquid chromatography.

REFERENCES

1. Prevalence of Fragile X Syndrome: <https://fragilex.org/understanding-fragile-x/fragile-x-101/prevalence/>. Accessed Oct. 20, 2018.
2. Penagarikano, O.; Mulle, J. G.; Warren, S. T., The pathophysiology of fragile x syndrome. *Annu. Rev. Genomics Hum. Genet.* **2007**, *8*, 109-29.
3. Khandjian, E. W.; Corbin, F.; Woerly, S.; Rousseau, F., The fragile X mental retardation protein is associated with ribosomes. *Nature Genet.* **1996**, *12*, 91-3.
4. Laggerbauer, B.; Ostareck, D.; Keidel, E. M.; Ostareck-Lederer, A.; Fischer, U., Evidence that fragile X mental retardation protein is a negative regulator of translation. *Hum. Mol. Genet.* **2001**, *10*, 329-38.
5. Darnell, J. C.; Van Driesche, S. J.; Zhang, C.; Hung, K. Y.; Mele, A.; Fraser, C. E.; Stone, E. F.; Chen, C.; Fak, J. J.; Chi, S. W.; Licatalosi, D. D.; Richter, J. D.; Darnell, R. B., FMRP stalls ribosomal translocation on mRNAs linked to synaptic function and autism. *Cell* **2011**, *146*, 247-61.
6. Bear, M. F.; Huber, K. M.; Warren, S. T., The mGluR theory of fragile X mental retardation. *Trends Neurosci.* **2004**, *27*, 370-7.
7. Michalon, A.; Sidorov, M.; Ballard, T. M.; Ozmen, L.; Spooren, W.; Wettstein, J. G.; Jaeschke, G.; Bear, M. F.; Lindemann, L., Chronic pharmacological mGlu5 inhibition corrects fragile X in adult mice. *Neuron* **2012**, *74*, 49-56.
8. Krueger, D. D.; Bear, M. F., Toward fulfilling the promise of molecular medicine in fragile X syndrome. *Annu. Rev. Med.* **2011**, *62*, 411-29.
9. Youssef, E. A.; Berry-Kravis, E.; Czech, C.; Hagerman, R. J.; Hessel, D.; Wong, C. Y.; Rabbia, M.; Deptula, D.; John, A.; Kinch, R.; Drewitt, P.; Lindemann, L.; Marcinowski, M.;

1
2
3 Langland, R.; Horn, C.; Fontoura, P.; Santarelli, L.; Quiroz, J. A.; FragXis Study, G., Effect of the
4 mGluR5-NAM Basimglurant on Behavior in Adolescents and Adults with Fragile X Syndrome in
5 a Randomized, Double-Blind, Placebo-Controlled Trial: FragXis Phase 2 Results.
6
7
8
9
10 *Neuropsychopharmacol.* **2017**, *43*, 503-12.

11
12 10. Scharf, S. H.; Jaeschke, G.; Wettstein, J. G.; Lindemann, L., Metabotropic glutamate
13 receptor 5 as drug target for Fragile X syndrome. *Curr. Opin. Pharmacol.* **2015**, *20*, 124-34.

14
15
16
17 11. Davenport, M. H.; Schaefer, T. L.; Friedmann, K. J.; Fitzpatrick, S. E.; Erickson, C. A.,
18 Pharmacotherapy for Fragile X Syndrome: Progress to Date. *Drugs* **2016**, *76*, 431-45.

19
20
21
22 12. Torrioli, M.; Vernacotola, S.; Setini, C.; Bevilacqua, F.; Martinelli, D.; Snape, M.;
23 Hutchison, J. A.; Di Raimo, F. R.; Tabolacci, E.; Neri, G., Treatment with valproic acid ameliorates
24 ADHD symptoms in fragile X syndrome boys. *Am. J. Med. Genet. A* **2010**, *152A*, 1420-7.

25
26
27
28 13. Tabolacci, E.; De Pascalis, I.; Accadia, M.; Terracciano, A.; Moscato, U.; Chiurazzi, P.;
29 Neri, G., Modest reactivation of the mutant FMR1 gene by valproic acid is accompanied by histone
30 modifications but not DNA demethylation. *Pharmacogenet. Genomics* **2008**, *18*, 738-41.

31
32
33
34 14. Penney, J.; Tsai, L. H., Histone deacetylases in memory and cognition. *Sci. Signal.* **2014**,
35
36
37
38
39 7, re12.

40
41
42
43 15. Guan, J. S.; Haggarty, S. J.; Giacometti, E.; Dannenberg, J. H.; Joseph, N.; Gao, J.; Nieland,
44
45
46
47
48
49
50
51
52
53
54
55
56
57
58
59
60
60 T. J.; Zhou, Y.; Wang, X.; Mazitschek, R.; Bradner, J. E.; DePinho, R. A.; Jaenisch, R.; Tsai, L.
H., HDAC2 negatively regulates memory formation and synaptic plasticity. *Nature* **2009**, *459*, 55-
60.

16. Kim, M. S.; Akhtar, M. W.; Adachi, M.; Mahgoub, M.; Bassel-Duby, R.; Kavalali, E. T.;
Olson, E. N.; Monteggia, L. M., An essential role for histone deacetylase 4 in synaptic plasticity
and memory formation. *J. Neurosci.* **2012**, *32*, 10879-86.

- 1
2
3 17. McQuown, S. C.; Barrett, R. M.; Matheos, D. P.; Post, R. J.; Rogge, G. A.; Alenghat, T.;
4
5 Mullican, S. E.; Jones, S.; Rusche, J. R.; Lazar, M. A.; Wood, M. A., HDAC3 is a critical negative
6
7 regulator of long-term memory formation. *J. Neurosci.* **2011**, *31*, 764-74.
8
9
10 18. Tang, B. L., Class II HDACs and neuronal regeneration. *J. Cell. Biochem.* **2014**, *115*, 1225-
11
12 33.
13
14 19. Pardo, M.; Cheng, Y.; Velmeshev, D.; Magistri, M.; Eldar-Finkelman, H.; Martinez, A.;
15
16 Faghihi, M. A.; Jope, R. S.; Beurel, E., Intranasal siRNA administration reveals IGF2 deficiency
17
18 contributes to impaired cognition in Fragile X syndrome mice. *JCI insight* **2017**, *2*, e91782.
19
20
21 20. de Ruijter, A. J.; van Gennip, A. H.; Caron, H. N.; Kemp, S.; van Kuilenburg, A. B.,
22
23 Histone deacetylases (HDACs): characterization of the classical HDAC family. *Biochem. J.* **2003**,
24
25 *370*, 737-49.
26
27
28 21. Boyault, C.; Sadoul, K.; Pabion, M.; Khochbin, S., HDAC6, at the crossroads between
29
30 cytoskeleton and cell signaling by acetylation and ubiquitination. *Oncogene* **2007**, *26*, 5468-76.
31
32
33 22. Matthias, P.; Yoshida, M.; Khochbin, S., HDAC6 a new cellular stress surveillance factor.
34
35 *Cell Cycle* **2008**, *7*, 7-10.
36
37
38 23. Li, T.; Zhang, C.; Hassan, S.; Liu, X.; Song, F.; Chen, K.; Zhang, W.; Yang, J., Histone
39
40 deacetylase 6 in cancer. *J. Hematol. Oncol.* **2018**, *11*, 111.
41
42
43 24. Perdiz, D.; Mackeh, R.; Pous, C.; Baillet, A., The ins and outs of tubulin acetylation: more
44
45 than just a post-translational modification? *Cell Signal* **2011**, *23*, 763-71.
46
47
48 25. Arce, C. A.; Casale, C. H.; Barra, H. S., Submembraneous microtubule cytoskeleton:
49
50 regulation of ATPases by interaction with acetylated tubulin. *FEBS J.* **2008**, *275*, 4664-74.
51
52
53
54
55
56
57
58
59
60

- 1
2
3 26. Hammond, J. W.; Huang, C. F.; Kaech, S.; Jacobson, C.; Banker, G.; Verhey, K. J.,
4 Posttranslational modifications of tubulin and the polarized transport of kinesin-1 in neurons. *Mol.*
5
6 *Biol. Cell* **2010**, *21*, 572-83.
7
8
9
10 27. Hirokawa, N.; Niwa, S.; Tanaka, Y., Molecular motors in neurons: transport mechanisms
11 and roles in brain function, development, and disease. *Neuron* **2010**, *68*, 610-38.
12
13
14 28. Gardiner, J.; Barton, D.; Marc, J.; Overall, R., Potential role of tubulin acetylation and
15 microtubule-based protein trafficking in familial dysautonomia. *Traffic* **2007**, *8*, 1145-9.
16
17
18
19 29. Liu, X. A.; Rizzo, V.; Puthanveetil, S. V., Pathologies of Axonal Transport in
20 Neurodegenerative Diseases. *Transl. Neurosci.* **2012**, *3*, 355-72.
21
22
23
24 30. Jochems, J.; Boulden, J.; Lee, B. G.; Blendy, J. A.; Jarpe, M.; Mazitschek, R.; Van Duzer,
25 J. H.; Jones, S.; Berton, O., Antidepressant-like properties of novel HDAC6-selective inhibitors
26 with improved brain bioavailability. *Neuropsychopharmacol.* **2014**, *39*, 389-400.
27
28
29
30 31. Wang, Z.; Leng, Y.; Wang, J.; Liao, H. M.; Bergman, J.; Leeds, P.; Kozikowski, A.;
31 Chuang, D. M., Tubastatin A, an HDAC6 inhibitor, alleviates stroke-induced brain infarction and
32 functional deficits: potential roles of alpha-tubulin acetylation and FGF-21 up-regulation. *Sci. Rep.*
33 **2016**, *6*, 19626.
34
35
36
37 32. Pinho, B. R.; Reis, S. D.; Guedes-Dias, P.; Leitao-Rocha, A.; Quintas, C.; Valentao, P.;
38 Andrade, P. B.; Santos, M. M.; Oliveira, J. M., Pharmacological modulation of HDAC1 and
39 HDAC6 in vivo in a zebrafish model: Therapeutic implications for Parkinson's disease. *Pharmacol.*
40 *Res.* **2016**, *103*, 328-39.
41
42
43
44 33. Zhang, L.; Liu, C.; Wu, J.; Tao, J. J.; Sui, X. L.; Yao, Z. G.; Xu, Y. F.; Huang, L.; Zhu, H.;
45 Sheng, S. L.; Qin, C., Tubastatin A/ACY-1215 improves cognition in Alzheimer's disease
46 transgenic mice. *J. Alzheimers Dis.* **2014**, *41*, 1193-205.
47
48
49
50
51
52
53
54
55
56
57
58
59
60

- 1
2
3 34. Zhang, L.; Sheng, S.; Qin, C., The role of HDAC6 in Alzheimer's disease. *J. Alzheimers*
4 *Dis.* **2013**, *33*, 283-95.
5
6
7
8 35. Selenica, M. L.; Benner, L.; Housley, S. B.; Manchec, B.; Lee, D. C.; Nash, K. R.; Kalin,
9 J.; Bergman, J. A.; Kozikowski, A.; Gordon, M. N.; Morgan, D., Histone deacetylase 6 inhibition
10 improves memory and reduces total tau levels in a mouse model of tau deposition. *Alzheimers Res.*
11 *Ther.* **2014**, *6*, 12.
12
13
14
15
16
17 36. d'Ydewalle, C.; Krishnan, J.; Chiheb, D. M.; Van Damme, P.; Irobi, J.; Kozikowski, A. P.;
18 Vanden Berghe, P.; Timmerman, V.; Robberecht, W.; Van Den Bosch, L., HDAC6 inhibitors
19 reverse axonal loss in a mouse model of mutant HSPB1-induced Charcot-Marie-Tooth disease.
20 *Nat. Med.* **2011**, *17*, 968-74.
21
22
23
24
25
26 37. Kim, J. Y.; Woo, S. Y.; Hong, Y. B.; Choi, H.; Kim, J.; Choi, H.; Mook-Jung, I.; Ha, N.;
27 Kyung, J.; Koo, S. K.; Jung, S. C.; Choi, B. O., HDAC6 Inhibitors Rescued the Defective Axonal
28 Mitochondrial Movement in Motor Neurons Derived from the Induced Pluripotent Stem Cells of
29 Peripheral Neuropathy Patients with HSPB1 Mutation. *Stem Cells Int.* **2016**, *2016*, 9475981.
30
31
32
33
34
35 38. Benoy, V.; Vanden Berghe, P.; Jarpe, M.; Van Damme, P.; Robberecht, W.; Van Den
36 Bosch, L., Development of Improved HDAC6 Inhibitors as Pharmacological Therapy for Axonal
37 Charcot-Marie-Tooth Disease. *Neurotherapeutics* **2017**, *14*, 417-28.
38
39
40
41
42 39. Gold, W. A.; Lacina, T. A.; Cantrill, L. C.; Christodoulou, J., MeCP2 deficiency is
43 associated with reduced levels of tubulin acetylation and can be restored using HDAC6 inhibitors.
44 *J. Mol. Med.* **2015**, *93*, 63-72.
45
46
47
48
49 40. Guo, W.; Naujock, M.; Fumagalli, L.; Vandoorne, T.; Baatsen, P.; Boon, R.; Ordovas, L.;
50 Patel, A.; Welters, M.; Vanwelden, T.; Geens, N.; Tricot, T.; Benoy, V.; Steyaert, J.; Lefebvre-
51 Omar, C.; Boesmans, W.; Jarpe, M.; Sternecker, J.; Wegner, F.; Petri, S.; Bohl, D.; Vanden
52
53
54
55
56
57
58
59
60

1
2
3 Berghe, P.; Robberecht, W.; Van Damme, P.; Verfaillie, C.; Van Den Bosch, L., HDAC6
4 inhibition reverses axonal transport defects in motor neurons derived from FUS-ALS patients. *Nat.*
5
6
7
8 *Comm.* **2017**, *8*, 861.

9
10 41. Ross-Inta, C.; Omanska-Klusek, A.; Wong, S.; Barrow, C.; Garcia-Arocena, D.; Iwahashi,
11 C.; Berry-Kravis, E.; Hagerman, R. J.; Hagerman, P. J.; Giulivi, C., Evidence of mitochondrial
12 dysfunction in fragile X-associated tremor/ataxia syndrome. *Biochem. J.* **2010**, *429*, 545-52.

13
14
15 42. Kaplan, E. S.; Cao, Z.; Hulsizer, S.; Tassone, F.; Berman, R. F.; Hagerman, P. J.; Pessah,
16 I. N., Early mitochondrial abnormalities in hippocampal neurons cultured from Fmr1 pre-mutation
17 mouse model. *J. Neurochem.* **2012**, *123*, 613-21.

18
19
20 43. Chen, S.; Owens, G. C.; Makarenkova, H.; Edelman, D. B., HDAC6 regulates
21 mitochondrial transport in hippocampal neurons. *PLoS One* **2010**, *5*, e10848.

22
23
24 44. Xu, X.; Kozikowski, A. P.; Pozzo-Miller, L., A selective histone deacetylase-6 inhibitor
25 improves BDNF trafficking in hippocampal neurons from Mecp2 knockout mice: implications for
26 Rett syndrome. *Front. Cell. Neurosci.* **2014**, *8*, 68.

27
28
29 45. Uutela, M.; Lindholm, J.; Louhivuori, V.; Wei, H.; Louhivuori, L. M.; Pertovaara, A.;
30 Akerman, K.; Castren, E.; Castren, M. L., Reduction of BDNF expression in Fmr1 knockout mice
31 worsens cognitive deficits but improves hyperactivity and sensorimotor deficits. *Genes Brain*
32 *Behav.* **2012**, *11*, 513-23.

33
34
35 46. Langley, B.; D'Annibale, M. A.; Suh, K.; Ayoub, I.; Tolhurst, A.; Bastan, B.; Yang, L.;
36 Ko, B.; Fisher, M.; Cho, S.; Beal, M. F.; Ratan, R. R., Pulse inhibition of histone deacetylases
37 induces complete resistance to oxidative death in cortical neurons without toxicity and reveals a
38 role for cytoplasmic p21(waf1/cip1) in cell cycle-independent neuroprotection. *J. Neurosci.* **2008**,
39
40
41
42
43
44
45
46
47
48
49
50
51
52
53
54
55
56
57
58
59
60
28, 163-76.

- 1
2
3 47. Riviuccio, M. A.; Brochier, C.; Willis, D. E.; Walker, B. A.; D'Annibale, M. A.;
4
5
6
7
8
9
10
11
12
13
14
15
16
17
18
19
20
21
22
23
24
25
26
27
28
29
30
31
32
33
34
35
36
37
38
39
40
41
42
43
44
45
46
47
48
49
50
51
52
53
54
55
56
57
58
59
60
47. Riviuccio, M. A.; Brochier, C.; Willis, D. E.; Walker, B. A.; D'Annibale, M. A.;
McLaughlin, K.; Siddiq, A.; Kozikowski, A. P.; Jaffrey, S. R.; Twiss, J. L.; Ratan, R. R.; Langley,
B., HDAC6 is a target for protection and regeneration following injury in the nervous system. *Proc.
Nat. Acad. Sci. U. S. A* **2009**, *106*, 19599-604.
48. Wang, X. X.; Wan, R. Z.; Liu, Z. P., Recent advances in the discovery of potent and
selective HDAC6 inhibitors. *Euro. J. Med. Chem.* **2018**, *143*, 1406-18.
49. Yee, A. J.; Bensinger, W. I.; Supko, J. G.; Voorhees, P. M.; Berdeja, J. G.; Richardson, P.
G.; Libby, E. N.; Wallace, E. E.; Birrer, N. E.; Burke, J. N.; Tamang, D. L.; Yang, M.; Jones, S.
S.; Wheeler, C. A.; Markelewicz, R. J.; Raje, N. S., Ricolinostat plus lenalidomide, and
dexamethasone in relapsed or refractory multiple myeloma: a multicentre phase 1b trial. *The
Lancet. Oncol.* **2016**, *17*, 1569-78.
50. Clinical trials for ACY-1215. <[https://clinicaltrials.gov/ct2/results?term=ACY-
1215&Search=Search](https://clinicaltrials.gov/ct2/results?term=ACY-1215&Search=Search)>. Accessed Sep. 28, 2018.
51. Clinical trials for ACY-241. <[https://clinicaltrials.gov/ct2/results?term=ACY-
241&Search=Search](https://clinicaltrials.gov/ct2/results?term=ACY-241&Search=Search)>. Accessed Sep. 28, 2018.
52. Lee, H. Y.; Fan, S. J.; Huang, F. I.; Chao, H. Y.; Hsu, K. C.; Lin, T. E.; Yeh, T. K.; Lai,
M. J.; Li, Y. H.; Huang, H. L.; Yang, C. R.; Liou, J. P., 5-Aroylindoles Act as Selective Histone
Deacetylase 6 Inhibitors Ameliorating Alzheimer's Disease Phenotypes. *J. Med. Chem.* **2018**, *61*,
7087-102.
53. Fan, S. J.; Huang, F. I.; Liou, J. P.; Yang, C. R., The novel histone de acetylase 6 inhibitor,
MPT0G211, ameliorates tau phosphorylation and cognitive deficits in an Alzheimer's disease
model. *Cell Death Dis.* **2018**, *9*, 655.

- 1
2
3 54. Yu, C. W.; Chang, P. T.; Hsin, L. W.; Chern, J. W., Quinazolin-4-one derivatives as
4 selective histone deacetylase-6 inhibitors for the treatment of Alzheimer's disease. *J. Med. Chem.*
5
6
7 **2013**, *56*, 6775-91.
8
9
- 10 55. Strebl, M. G.; Campbell, A. J.; Zhao, W. N.; Schroeder, F. A.; Riley, M. M.; Chindavong,
11 P. S.; Morin, T. M.; Haggarty, S. J.; Wagner, F. F.; Ritter, T.; Hooker, J. M., HDAC6 Brain
12 Mapping with [(18)F]Bavarostat Enabled by a Ru-Mediated Deoxyfluorination. *ACS Cent. Sci.*
13
14 **2017**, *3*, 1006-14.
15
16
17
- 18 56. Wager, T. T.; Chandrasekaran, R. Y.; Hou, X.; Troutman, M. D.; Verhoest, P. R.;
19 Villalobos, A.; Will, Y., Defining desirable central nervous system drug space through the
20 alignment of molecular properties, in vitro ADME, and safety attributes. *ACS Chem. Neurosci.*
21
22 **2010**, *1*, 420-34.
23
24
25
- 26 57. Wager, T. T.; Hou, X.; Verhoest, P. R.; Villalobos, A., Moving beyond rules: the
27 development of a central nervous system multiparameter optimization (CNS MPO) approach to
28 enable alignment of druglike properties. *ACS Chem. Neurosci.* **2010**, *1*, 435-49.
29
30
31
32
33
- 34 58. Wager, T. T.; Hou, X.; Verhoest, P. R.; Villalobos, A., Central Nervous System
35 Multiparameter Optimization Desirability: Application in Drug Discovery. *ACS Chem. Neurosci.*
36
37 **2016**, *7*, 767-75.
38
39
40
41
- 42 59. Porter, N. J.; Mahendran, A.; Breslow, R.; Christianson, D. W., Unusual zinc-binding mode
43 of HDAC6-selective hydroxamate inhibitors. *Proc. Nat. Acad. Sci. U. S. A.* **2017**, *114*, 13459-64.
44
45
46
- 47 60. Wagner, F. F.; Olson, D. E.; Gale, J. P.; Kaya, T.; Weiwer, M.; Aidoud, N.; Thomas, M.;
48 Davoine, E. L.; Lemercier, B. C.; Zhang, Y. L.; Holson, E. B., Potent and selective inhibition of
49 histone deacetylase 6 (HDAC6) does not require a surface-binding motif. *J. Med. Chem.* **2013**, *56*,
50
51
52
53
54
55
56
57
58
59
60

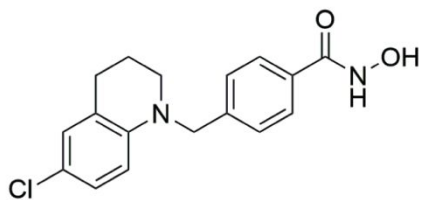
- 1
2
3 61. Porter, N. J.; Wagner, F. F.; Christianson, D. W., Entropy as a Driver of Selectivity for
4 Inhibitor Binding to Histone Deacetylase 6. *Biochemistry* **2018**, *57*, 3916-24.
5
6
7
8 62. Shen, S.; Benoy, V.; Bergman, J. A.; Kalin, J. H.; Frojuello, M.; Vistoli, G.; Haeck, W.;
9 Van Den Bosch, L.; Kozikowski, A. P., Bicyclic-Capped Histone Deacetylase 6 Inhibitors with
10 Improved Activity in a Model of Axonal Charcot-Marie-Tooth Disease. *ACS Chem. Neurosci.*
11 **2016**, *7*, 240-58.
12
13
14
15
16
17 63. Gaisina, I. N.; Lee, S. H.; Kaidery, N. A.; Ben Aissa, M.; Ahuja, M.; Smirnova, N. N.;
18 Wakade, S.; Gaisin, A.; Bourassa, M. W.; Ratan, R. R.; Nikulin, S. V.; Poloznikov, A. A.; Thomas,
19 B.; Thatcher, G. R. J.; Gazaryan, I. G., Activation of Nrf2 and Hypoxic Adaptive Response
20 Contribute to Neuroprotection Elicited by Phenylhydroxamic Acid Selective HDAC6 Inhibitors.
21 *ACS Chem. Neurosci.* **2018**, *9*, 894-900.
22
23
24
25
26
27
28 64. Bergman, J. A.; Woan, K.; Perez-Villaruel, P.; Villagra, A.; Sotomayor, E. M.;
29 Kozikowski, A. P., Selective histone deacetylase 6 inhibitors bearing substituted urea linkers
30 inhibit melanoma cell growth. *J. Med. Chem.* **2012**, *55*, 9891-9.
31
32
33
34
35 65. Robers, M. B.; Dart, M. L.; Woodroffe, C. C.; Zimprich, C. A.; Kirkland, T. A.; Machleidt,
36 T.; Kupcho, K. R.; Levin, S.; Hartnett, J. R.; Zimmerman, K.; Niles, A. L.; Ohana, R. F.; Daniels,
37 D. L.; Slater, M.; Wood, M. G.; Cong, M.; Cheng, Y. Q.; Wood, K. V., Target engagement and
38 drug residence time can be observed in living cells with BRET. *Nat. Comm.* **2015**, *6*, 10091.
39
40
41
42
43
44 66. Jin, X.; Luong, T. L.; Reese, N.; Gaona, H.; Collazo-Velez, V.; Vuong, C.; Potter, B.;
45 Sousa, J. C.; Olmeda, R.; Li, Q.; Xie, L.; Zhang, J.; Zhang, P.; Reichard, G.; Melendez, V.;
46 Marcsisin, S. R.; Pybus, B. S., Comparison of MDCK-MDR1 and Caco-2 cell based permeability
47 assays for anti-malarial drug screening and drug investigations. *J. Pharmacol. Toxicol. Methods*
48 **2014**, *70*, 188-94.
49
50
51
52
53
54
55
56
57
58
59
60

- 1
2
3 67. Wang, Q.; Rager, J. D.; Weinstein, K.; Kardos, P. S.; Dobson, G. L.; Li, J.; Hidalgo, I. J.,
4 Evaluation of the MDR-MDCK cell line as a permeability screen for the blood-brain barrier. *Int.*
5
6 *J. Pharmaceut.* **2005**, *288*, 349-59.
7
8
9
10 68. Ghose, A. K.; Herbertz, T.; Hudkins, R. L.; Dorsey, B. D.; Mallamo, J. P., Knowledge-
11
12 Based, Central Nervous System (CNS) Lead Selection and Lead Optimization for CNS Drug
13
14 Discovery. *ACS Chem. Neurosci.* **2012**, *3*, 50-68.
15
16
17 69. Tam, K. Y.; Avdeef, A.; Tsinman, O.; Sun, N., The permeation of amphoteric drugs
18
19 through artificial membranes--an in combo absorption model based on paracellular and
20
21 transmembrane permeability. *J. Med. Chem.* **2010**, *53*, 392-401.
22
23
24 70. Wu, Y. J.; Guernon, J.; McClure, A.; Luo, G.; Rajamani, R.; Ng, A.; Easton, A.; Newton,
25
26 A.; Bourin, C.; Parker, D.; Mosure, K.; Barnaby, O.; Soars, M. G.; Knox, R. J.; Matchett, M.;
27
28 Pieschl, R.; Herrington, J.; Chen, P.; Sivarao, D. V.; Bristow, L. J.; Meanwell, N. A.; Bronson, J.;
29
30 Olson, R.; Thompson, L. A.; Dzierba, C., Discovery of non-zwitterionic aryl sulfonamides as
31
32 Nav1.7 inhibitors with efficacy in preclinical behavioral models and translational measures of
33
34 nociceptive neuron activation. *Bioorg. Med. Chem.* **2017**, *25*, 5490-505.
35
36
37 71. Hamdouchi, C.; Maiti, P.; Warshawsky, A. M.; DeBaillie, A. C.; Otto, K. A.; Wilbur, K.
38
39 L.; Kahl, S. D.; Patel Lewis, A.; Cardona, G. R.; Zink, R. W.; Chen, K.; Cr, S.; Lineswala, J. P.;
40
41 Neathery, G. L.; Bouaichi, C.; Diseroad, B. A.; Campbell, A. N.; Sweetana, S. A.; Adams, L. A.;
42
43 Cabrera, O.; Ma, X.; Yumibe, N. P.; Montrose-Rafizadeh, C.; Chen, Y.; Miller, A. R., Discovery
44
45 of LY3104607: A Potent and Selective G Protein-Coupled Receptor 40 (GPR40) Agonist with
46
47 Optimized Pharmacokinetic Properties to Support Once Daily Oral Treatment in Patients with
48
49 Type 2 Diabetes Mellitus. *J. Med. Chem.* **2018**, *61*, 934-45.
50
51
52
53
54
55
56
57
58
59
60

- 1
2
3 72. Shen, S.; Kozikowski, A. P., Why Hydroxamates May Not Be the Best Histone
4 Deacetylase Inhibitors--What Some May Have Forgotten or Would Rather Forget?
5
6 *ChemMedChem* **2016**, *11*, 15-21.
7
8
9
10 73. Pieretti, M.; Zhang, F. P.; Fu, Y. H.; Warren, S. T.; Oostra, B. A.; Caskey, C. T.; Nelson,
11 D. L., Absence of expression of the FMR-1 gene in fragile X syndrome. *Cell* **1991**, *66*, 817-22.
12
13
14 74. Fmr1 knockout mice: a model to study fragile X mental retardation. The Dutch-Belgian
15 Fragile X Consortium. *Cell* **1994**, *78*, 23-33.
16
17
18
19 75. Franklin, A. V.; King, M. K.; Palomo, V.; Martinez, A.; McMahon, L. L.; Jope, R. S.,
20 Glycogen synthase kinase-3 inhibitors reverse deficits in long-term potentiation and cognition in
21 fragile X mice. *Biol. Psychiatry* **2014**, *75*, 198-206.
22
23
24
25
26 76. Yuskaitis, C. J.; Mines, M. A.; King, M. K.; Sweatt, J. D.; Miller, C. A.; Jope, R. S.,
27 Lithium ameliorates altered glycogen synthase kinase-3 and behavior in a mouse model of fragile
28 X syndrome. *Biochem. Pharmacol.* **2010**, *79*, 632-46.
29
30
31
32
33 77. Wang, X. X.; Wan, R. Z.; Liu, Z. P., Recent advances in the discovery of potent and
34 selective HDAC6 inhibitors. *Euro. J. Med. Chem.* **2018**, *143*, 1406-18.
35
36
37
38 78. Li, L.; Yang, X. J., Tubulin acetylation: responsible enzymes, biological functions and
39 human diseases. *Cell Mol. Life Sci.* **2015**, *72*, 4237-55.
40
41
42
43 79. Taes, I.; Timmers, M.; Hersmus, N.; Bento-Abreu, A.; Van Den Bosch, L.; Van Damme,
44 P.; Auwerx, J.; Robberecht, W., Hdac6 deletion delays disease progression in the SOD1G93A
45 mouse model of ALS. *Hum. Mol. Genet.* **2013**, *22*, 1783-90.
46
47
48
49 80. Fernandez-Barrera, J.; Correas, I.; Alonso, M. A., Age-related neuropathies and tubulin
50 acetylation. *Aging (Albany NY)* **2018**, *10*, 524-25.
51
52
53
54
55
56
57
58
59
60

- 1
2
3 81. Erck, C.; Peris, L.; Andrieux, A.; Meissirel, C.; Gruber, A. D.; Vernet, M.; Schweitzer, A.;
4 Saoudi, Y.; Pointu, H.; Bosc, C.; Salin, P. A.; Job, D.; Wehland, J., A vital role of tubulin-tyrosine-
5
6 ligase for neuronal organization. *Proc. Nat. Acad. Sci. U. S. A.* **2005**, *102*, 7853-8.
7
8
9
10 82. Ventura, R.; Pascucci, T.; Catania, M. V.; Musumeci, S. A.; Puglisi-Allegra, S., Object
11
12 recognition impairment in Fmr1 knockout mice is reversed by amphetamine: involvement of
13
14 dopamine in the medial prefrontal cortex. *Behav. Pharmacol.* **2004**, *15*, 433-42.
15
16
17 83. Pacey, L. K.; Tharmalingam, S.; Hampson, D. R., Subchronic administration and
18
19 combination metabotropic glutamate and GABAB receptor drug therapy in fragile X syndrome. *J.*
20
21 *Pharmacol. Exp. Ther.* **2011**, *338*, 897-905.
22
23
24 84. Eadie, B. D.; Cushman, J.; Kannangara, T. S.; Fanselow, M. S.; Christie, B. R., NMDA
25
26 receptor hypofunction in the dentate gyrus and impaired context discrimination in adult Fmr1
27
28 knockout mice. *Hippocampus* **2012**, *22*, 241-54.
29
30
31 85. King, M. K.; Jope, R. S., Lithium treatment alleviates impaired cognition in a mouse model
32
33 of fragile X syndrome. *Genes Brain Behav.* **2013**, *12*, 723-31.
34
35
36 86. Miyake, Y.; Keusch, J. J.; Wang, L.; Saito, M.; Hess, D.; Wang, X.; Melancon, B. J.;
37
38 Helquist, P.; Gut, H.; Matthias, P., Structural insights into HDAC6 tubulin deacetylation and its
39
40 selective inhibition. *Nat. Chem. Biol.* **2016**, *12*, 748-54.
41
42
43 87. Pardo, M.; King, M. K.; Perez-Costas, E.; Melendez-Ferro, M.; Martinez, A.; Beurel, E.;
44
45 Jope, R. S., Impairments in cognition and neural precursor cell proliferation in mice expressing
46
47 constitutively active glycogen synthase kinase-3. *Front. Behav. Neurosci.* **2015**, *9*, 55.
48
49
50 88. Bradford, M. M., A rapid and sensitive method for the quantitation of microgram quantities
51
52 of protein utilizing the principle of protein-dye binding. *Anal. Biochem.* **1976**, *72*, 248-54.
53
54
55
56
57
58
59
60

Graphic Abstract

**SW-100**HDAC1, $IC_{50} = 5.3 \mu\text{M}$ P-gp efflux ratio = 0.5HDAC8, $IC_{50} = 3.7 \mu\text{M}$ B/P = 2.54 @1 hHDAC6, $IC_{50} = 2.3 \text{ nM}$ 4.54 @4 h